NASA Technical Memorandum 106728

Experimental Investigation of the Performance of a Mach-2.7 Two-Dimensional Bifurcated Duct Inlet With 30 Percent Internal Contraction

Joseph F. Wasserbauer, Edward T. Meleason,
and Paul L. Burstadt
Lewis Research Center
Cleveland, Ohio

May 1996

National Aeronautics and
Space Administration

EXPERIMENTAL INVESTIGATION OF THE PERFORMANCE OF A MACH-2.7 TWO-DIMENSIONAL BIFURCATED DUCT INLET WITH 30 PERCENT INTERNAL CONTRACTION

Joseph F. Wasserbauer, Edward T. Meleason, and Paul L. Burstadt
National Aeronautics and Space Administration
Lewis Research Center
Cleveland, Ohio 44135

SUMMARY

An experimental study was conducted to determine the performance of a two-dimensional, mixed-compression bifurcated duct inlet system designed for a free-stream Mach number of 2.7. Thirty percent of the supersonic area contraction occurred internally. A movable ramp was used to vary the contraction ratio for off-design operation. Boundary layer bleed regions were located on the cowl, centerbody, and sidewall surfaces. There were also provisions for vortex generators on the cowl and centerbody of the subsonic diffuser.

Data were obtained over the Mach number range of 2.0 to 2.8 and at angles of yaw from 0° to the maximum value prior to inlet unstart. The test at Mach 2.8 was to obtain data for an over-speed condition. The Reynolds number varied from 2.5 to 2.3 million/ft for Mach numbers above 2.5. At Mach numbers of 2.5 and lower, the Reynolds number was set at 2.5 million/ft. Bleed patterns, vortex generator patterns, and ramp position were varied, and three inlet configurations were selected for more extensive study. Two of these configurations had self-starting capability.

One of the self-starting configurations produced 89 percent total pressure recovery at the compressor face station with 6.8 percent total bleed. The compressor face distortion was about 16 percent. Vortex generators were extremely effective in redistributing flow but were not as effective in reducing distortion.

Excellent flow symmetry was achieved between the separated halves of the inlet, and twin-duct instability was not observed. The ramp tip shock was steeper than expected. This caused the cowl lip shock to be reflected from the ramp instead of being cancelled at the shoulder. However, peak recovery at the throat was still obtained with the ramp near the design position.

INTRODUCTION

The NASA Lewis Research Center has been conducting an experimental program to evaluate and improve the performance characteristics of a family of supersonic inlet systems. The inlet systems investigated cover a range of geometries and compression splits. The results of this general research are intended to provide inlet performance criteria that could be used in the design and definition of future supersonic propulsion systems. Previous investigations in this program are discussed in references 1 to 4. Other investigations of a similar nature are covered in references 5 and 6.

This report presents the results of an investigation of a large-scale, two-dimensional inlet designed to provide the high performance needed for a supersonic aircraft at a cruise Mach number of 2.7 (fig. 1). A twin-duct, mixed (internal and external)-compression inlet design with variable forward ramp angles was used (see fig. 1(a)). Porous internal surfaces were provided for boundary layer bleed, and provisions for vortex generators were also included in the subsonic diffuser. The ramp tip shock was followed by a region of isentropic compression and the cowl lip shock was intended to intersect the ramp at the shoulder and be cancelled at that point. A discussion of the characteristic design of the inlet is given in reference 7.

The inlet performance was evaluated for several bleed locations, patterns, and flow rates. A series of vortex generator patterns and ramp positions were also investigated. Three inlet configurations were selected for more extensive study. Results are presented principally in terms of inlet total pressure recovery and distortion versus total bleed mass flow for a range of Mach numbers and yaw angles. The yaw angle variation is defined as the model pitch plane for the inlet mounted in the tunnel with the ramp leading edge in the horizontal position. At the design Mach number and 0° yaw angle, internal static pressure profiles for a series of terminal shock positions are presented.

The test was conducted in the Lewis 10-by 10-Foot Supersonic Wind Tunnel over a Mach number range of 2.0 to 2.8 and a Reynolds number range of 2.5 to 2.3 million/ft.

SYMBOLS

A	flow area
A_c	capture area, 343.178 in.^{2} (2.383 ft^2)
b_{VG}	vortex generator height, 0.60 in.
D_s	distance from cowl shock impingement to ramp shoulder
D_5	compressor face distortion, $(P_{max} - P_{min})/P_5$
h	height
h_c	cowl leading edge height from model centerline, 10.45 in.
h_D	design throat height
M	Mach number
M_s	surface Mach number
M_l	local Mach number
M_0	free-stream Mach number
m_o	capture mass flow
m_{sp}	spillage mass flow
m/m_o	mass-flow ratio
m_b/m_o	bleed mass-flow ratio
m_{btot}/m_o	total bleed mass-flow ratio
$(m_{th}/m_o)_{cr}$	critical throat bleed mass-flow ratio
m_5/m_o	compressor face mass-flow ratio
P	total pressure
P_l	local total pressure
P_{avg}	average compressor face total pressure
P_0	free-stream total pressure
P_{max}	maximum compressor face total pressure
P_{min}	minimum compressor face total pressure
P_{pl}	bleed plenum total pressure
P_5	average total pressure at compressor face
ΔP_{rms}	root-mean-square fluctuating component of total pressure

p	static pressure
p_s	surface static pressure
p_0	free-stream static pressure
R_{VG}	vortex generator leading edge radius
r	radius from model centerline
v_l/v_0	local velocity ratio
x	axial distance from ramp leading edge
y	vertical distance from model centerline
z	horizontal distance from model centerline
β	angle of yaw
β_{uns}	unstart angle of yaw
δ	ramp position, deg
θ	slope of surface

APPARATUS AND PROCEDURE

The inlet used in this investigation was a two-dimensional, mixed-compression bifurcated duct inlet system with a wedge-type variable ramp centerbody designed for a free-stream Mach number of 2.7. A cross-sectional view of the inlet is presented in figure 1(a). At the design Mach number, 30 percent of the supersonic area contraction occurred internally. The movable ramps were used to vary the contraction ratio for off-design operation. The inlet was attached to a nacelle containing either a J-85/13 turbojet engine or a choked exit plug assembly to vary the inlet airflow. Each duct is equipped with bleed ports and vortex generators located on the centerbody, cowl, and sidewalls. In addition, each duct is equipped with a pair of overboard bypass doors (located on the cowl) downstream of the geometric throat.

The overall length of the supersonic diffuser of the inlet is approximately one-half that of a single-duct inlet that supplies the same total airflow to the engine. Thus, the inlet can be conveniently mounted under the wing, which shields the inlet during high angle-of-attack maneuvers. The inlet would be mounted with the ramp in a vertical position so that maximum tolerance to sideslip could be achieved by varying the ramp position. The installation of the inlet model in the 10- by 10-Foot Supersonic Wind Tunnel is shown in figure 1(b). The inlet nacelle combination is mounted from a vertical strut in the wind tunnel test section. The bulge in the nacelle was required to house the engine accessory package. For this investigation the inlet was coupled to a cold-pipe choked exit plug assembly. As seen from figure 1(b), the inlet was mounted in the tunnel with the ramp in a horizontal position. Therefore, inlet tolerance to sideslip could be investigated by varying the pitch angle of the inlet.

Elements of the aerodynamic design, the centerline coordinates of the cowl and centerbody, are presented in table I. An isometric view of the inlet is shown in figure 1(c). Illustrated in the figure are the bleed regions and bleed ducts that were terminated by calibrated mass-flow plugs. The centerbody bleed regions were separated by sealed baffles. The ramp system was remotely actuated (expanded or collapsed) by hydraulic cylinders. An ejector bypass was located in the bypass door cavity. This bypass permits airflow past the engine for cooling purposes when engine inlet tests are conducted. The overboard bypass system consisted of four slotted sliding plate doors, two doors for each duct. The doors were individually controlled by electrohydraulic servomechanisms and were capable of bypassing approximately 88.5 percent of the duct airflow at the design Mach number. Vortex generators were installed on the cowl and aft ramps.

Details of the bleed regions and bleed patterns are shown in figure 1(d). The inlet performance bleed system was used for boundary layer control and increased stability. The bleed regions consisted of rows of holes (0.125 in. in diam) on the ramp, cowl, and sidewall surfaces. The forward ramp bleed was ducted overboard through pipes, as shown

in figure 1(c). The throat bleed (all surfaces) was ducted to a common plenum and then dumped overboard through four pipes (two of which can be seen in fig. 1(c)). The exit area of the pipes could be varied by remotely controlled plugs, thus allowing the throat bleed system to be backpressured.

Provisions were made for installing vortex generators on the cowl, ramp, and sidewall just aft of the throat region. Details of the vortex generators are shown in figure 1(e). The basic generator shape used was from the complete NACA 0012 airfoil. The radius of the leading edge was 0.012 in. and the generator height was 0.60 in., about equal to the local boundary layer height. The generators could be used as counter-rotating or co-rotating pairs.

The inlet design contours were obtained by using an inviscid method-of-characteristics solution (ref. 7). Details of the inlet characteristic design are shown in figures 1(f) and (g). The theoretical shock structure is shown in figure 1(f). The initial shock is followed by an isentropic compression fan. The cowl shock is designed for cancellation on the ramp shoulder followed by an isentropic compression region on the cowl and ramp centerbody to the throat station. The theoretical surface static pressure and Mach number distributions are shown in figure 1(g). The design throat Mach number is 1.3.

Static pressure measurements were made on the cowl and ramp surfaces, and their locations are listed in table II. The total pressures at the compressor face were measured by steady state and dynamic total-pressure-probe rakes (fig. 2(a)). Boundary layer rakes were located on the ramp shoulder and inlet sidewall near the throat region (fig. 2(b)). Total-pressure rakes were also located just aft of the throat in the corner of the cowl sidewall and in the corner of the ramp sidewall (fig. 2(c)).

The internal area distributions for several ramp positions are plotted in figure 3(a). The variation of the cowl contour in the subsonic diffuser from the geometric throat to the engine face is shown in figure 3(b). The transverse cowl coordinate dimensions at the model station transverse planes in figure 3(b) are presented in table III.

RESULTS

A schlieren photo of the inlet shock structure is shown in figure 4(a). The ramp tip shock, identified near the cowl lip, was steeper than anticipated. At a free-stream Mach number of 2.68, the ramp tip shock angle should be 25.7°. The shock angle measured from the schlieren photograph is a 26.3° angle, indicating more compression of the ramp flow field than design. The shock identified in the figure as sidewall spillage shock results from the sidewall boundary layer spilling over the leading edge of the ramp side plate. This spillage was a result of the ramp compression fan-sidewall boundary layer interaction. The net effect was about a 4- to 5-percent spillage mass-flow ratio. Figure 4 (b) shows the effect of free-stream Mach number on spillage for two ramp positions. Spillage over the cowl was less when the ramp angle δ was decreased from 15.81° (or when the throat height was increased).

An effort was made to determine the impingement of the cowl shock on the ramp centerbody with a cowl shock position rake as shown in figure 5(a). The theoretical and experimental shock positions are compared in figure 5(b) at a free-stream Mach number of 2.68 and a ramp angle of 15.81°. As seen in figure 5(b), the cowl shock impinges on the ramp ahead of the ramp shoulder where the shock is intended to be cancelled. Figure 5(c) shows the theoretical variation of the shock impingement on the ramp as the throat height is varied for various Mach numbers. The variation of total pressure recovery with throat height at Mach 2.68 is shown in figure 5(d) for various throat bleed mass-flow ratios. The steeper ramp shock structure, and the resulting increased compression, destroyed the theoretical shock pattern (fig. 1(f)). This caused the cowl lip shock to reflect from the ramp rather than cancel at the shoulder. However, total pressure recovery was still quite good. In fact, figure 5(d) shows that recovery is best at or below the design throat height h_D rather than at $h/h_D = 1.05$ where the cowl shock hits the ramp shoulder.

It was postulated that the ramp compression fan-sidewall boundary layer interaction steepens the ramp compression fan, resulting in an increase of the ramp compression ratio. This results in a lower Mach number downstream of the ramp compression and steepens the cowl lip shock. Thus, the cowl lip shock impinges on the ramp ahead of the ramp shoulder and is reflected rather than cancelled.

The effects of variations in bleed patterns for the forward ramps and sidewalls at the design Mach number of 2.68 are described in the vicinity of cowl lip shock (fig. 6). A summary of the bleed pattern configurations, their bleed mass-flow rates, and their supercritical unstart yaw angle tolerances, are presented in figure 6(a). The effect of bleed variation on ramp boundary layer and comparisons of ramp boundary layer profiles before and after the ramp shoulder are presented in figures 6(b) and (c), respectively. The effect of bleed variation on the sidewall boundary layer is shown in figure 6(d).

Based on figure 6(a), bleed configurations RS-2 and FS-2 were selected for supercritical inlet unstart yaw angles of 2.3° to 2.4°. Figure 6(a) shows the sensitivity of the inlet unstart yaw angle to the aft ramp bleed. This sensitivity can be seen by comparing configurations RS-3 and RS-4 with the same sidewall bleed. The effect of forward sidewall bleed is seen by comparing FS-2 and FS-3 with the same ramp bleed.

A summary of the effect of mid-diffuser bleed variations on the supercritical unstart yaw angle tolerance at the design Mach number of 2.68 is presented in figure 7. The comparisons show the effect of changing ramp and corner bleed patterns; as a result, the combination of FS-2 and MD-3 were selected.

The effect of the configuration throat bleed variation on inlet performance is presented in figure 8. The throat bleed configurations are shown in figure 8(a). In figure 8(b), the cowl corner rake describes the corner flow profiles for the various cowl corner throat bleed configurations of figure 8(a). The corner bleed configuration described for configuration TB-1 showed the most improved profiles (fig. 8(b)). For the ramp corner flow profiles, the configuration described for configuration TB-1 showed the best profile. The solid symbols in the figure denote the average midthroat recovery. The total pressure recovery performance for the throat bleed configurations is shown in figure 8(c). The throat bleed configurations were not backpressured during this series. The difference in total pressure recovery between configurations TB-1 and TB-3 is 0.5 percent at critical inlet operation (terminal shock at the geometric throat position). However, there is an increase in the total bleed mass-flow ratio of 2.25 percent required to obtain the increased pressure recovery of configuration TB-3.

The variation of the compressor face distortion with the total bleed mass-flow ratio for the various throat bleed configurations is shown in figure 8(d). At the critical operating condition for each throat bleed configuration, the lowest distortion was exhibited by configuration TB-3 with a value of 12.7 percent. Configuration TB-1 shows 16.7 percent distortion and configuration TB-2 shows 20.3 percent distortion. Configuration TB-1 was selected as the throat bleed configuration because there was only a difference of 0.5 percent in pressure recovery but a difference of 2.25 percent in the bleed mass-flow ratio.

The performance of the selected throat bleed configuration (TB-1) for various amounts of throat bleed mass-flow ratios at critical conditions is shown in figure 9. The throat bleed mass-flow ratio was varied by pressurizing the bleed plenum with the throat bleed mass-flow plugs. The inlet performance of the total pressure recovery and distortion versus the total bleed mass-flow ratio is shown in figure 9. A critical bleed mass-flow ratio of 0.055 for the throat bleed shows the best performance. At critical operating conditions and a throat bleed mass-flow ratio of 0.055, the distortion was 16.2 percent. Based on the results of figure 9, a throat bleed mass-flow ratio of 0.055 at critical inlet operation was selected.

The effect of vortex generators on the compressor face total-pressure contours is shown in figure 10 for configuration TB-1. With no vortex generators, low total pressures are exhibited on both cowl regions and corner regions (fig. 10(a)). When a full set of opposed pairs of vortex generators are used, the lower total pressures move to the sidewall and corner regions (fig. 10(b)). With only conventional opposed generator pairs on the cowl and in the corners (fig. 10(c)), a more even distribution of the total-pressure contours was obtained although the overall distortion value changed little. When parallel generators were used on the cowl and corner regions, improvement in the total-pressure contours was obtained (fig. 10(d)). A final generator pattern was tried: pairs of parallel generators on the cowl and conventional pairs on the ramp while the corner generators were maintained (fig. 10(e)). This pattern appeared to be the most effective in distributing flow. In general, the generator patterns investigated redistributed the flow but the improvement in distortion was not great. Parallel (co-rotating) generator pairs were more effective on the cowl than conventional opposed (counter-rotating) pairs. For the rest of the test, the pattern shown in figure 10(e) was selected.

The effect of the selected vortex generator pattern on overall inlet performance is shown in figure 11. The most obvious reduction is for dynamic distortion at supercritical shock positions. The reduction of steady state distortion near critical is apparent but not large.

The final inlet configuration selected, showing bleed patterns and the vortex generator pattern, is presented in figure 12. For the bleed and vortex generator patterns shown, SS-1 and SS-2 are self-starting configurations whereas NSS is not. The self-starting feature of an inlet during an inlet unstart sequence requires no variation in the inlet throat geometry to restart the inlet. Even though the inlet may have a self-start capability, inlet unstarts are to be avoided as much as possible. The bleed configurations for SS-2 and NSS are the same. The self-starting of SS-2 is accomplished by reducing the ramp angle from a design value of 15.81° to a value of 15.2°. Inlet configurations SS-1 and NSS use the design ramp angle. Here, inlet configuration SS-1 represents the bleed patterns needed for self-starting while using the design ramp position.

The overall inlet performance of the final configurations is shown in figure 13. Figure 13(a) shows the inlet pressure recovery and distortion is presented in figure 13(b).

The variation of the bleed mass-flow ratio versus the bleed plenum pressures for the bleeds on the ramp shoulder, forward sidewall, mid-diffuser, and throat is shown in figure 14 for the final inlet configurations. Although configurations NSS and SS-2 have the same bleed patterns, the difference in ramp angle causes a change in performance of the ramp shoulder and the forward sidewall bleeds.

A comparison of the twin-duct static pressure profiles at the design Mach number for inlet configuration SS-1 is presented in figure 15. The ramp profiles are shown in figure 15(a) and the cowl profiles are shown in figure 15(b). As seen in the figures, excellent symmetry between the separated halves of the inlet was obtained.

Inlet duct static pressure profiles for the final inlet configurations NSS, SS-1, and SS-2 at the design Mach number are presented in figures 16(a) and (b), (c) and (d), and (e) and (f), respectively. The static pressure profiles are shown for various total pressure recoveries and shock positions. The square symbols in each of the figures represent the critical inlet operation. As seen in the figures, the initial cowl static pressure profile is very close to theoretical, but the initial rise on the ramp is higher than the theoretical prediction for configurations NSS and SS-1. For configuration SS-2, the reduced ramp angle appears to remove the initial over-pressure on the ramp.

The inlet overall performance at off-design Mach numbers is shown for inlet configurations SS-1 and SS-2 in figure 17. The off-design Mach number performance for inlet configuration NSS is not presented because the performance of configurations SS-2 and NSS are the same at off-design conditions.

The effect of yaw angle on inlet performance at design Mach number conditions is presented in figures 18(a) to (c) for inlet configurations NSS, SS-1, and SS-2, respectively. The data shown are for windward and leeward ducts as well as for the full compressor face.

CONCLUDING REMARKS

1. A self-starting configuration that was developed produced 89 percent pressure recovery with 7 percent bleed. Higher recoveries could be achieved by increasing bleed or reducing the ramp throat height.

2. The ramp tip shock was steeper than anticipated and was a result of the ramp compression fan-sidewall boundary layer interaction steepening the ramp compression fan and increasing the compression pressure ratio. The net effect was about a 4- to 5-percent spillage mass flow.

3. The steeper shock structure deviated from the theoretical shock pattern, but the throat recovery was still good. The cowl lip shock was not cancelled but was reflected. However, peak recovery occurred near the design throat height despite the strong shock reflection from the ramp.

4. Bleed ahead of the throat affected the angle-of-yaw tolerance and self-starting. Bleed in the vicinity of the cowl lip shock was the most influential on the angle-of-yaw capability whereas the bleed between the ramp shoulder and the throat significantly affected self-starting. An angle-of-yaw angle tolerance of 3° to 4° was obtained.

5. Extra bleed in the corners was helpful. In the throat region, bleed areas with high porosity and high backpressure were more effective than similar patterns with low porosity and choked holes. A throat bleed of 4.5 to 5 percent was required for good performance.

6. High steady state distortions were generally obtained. For configurations without vortex generators, large regions of separated flow were present at the compressor face.

7. Vortex generators were extremely effective in redistributing the flow, but the improvement in distortion was not great. Parallel, or co-rotating, generator pairs were more effective on the cowl than opposed, or counter-rotating pairs.

8. Two inlet configurations had self-starting capabilities. Configuration SS-1 had self-start capability at the design ramp position of 15.81° whereas configuration SS-2 demonstrated self-start at a reduced ramp angle of 15.2°.

REFERENCES

1. Cubbison, Robert, W.; Meleason, Edward, T.; and Johnson, David, F.: Effect of Porous Bleed in a High-Performance Axisymmetric, Mixed-Compression Inlet at Mach 2.50. NASA TM X–1692, 1968.
2. Cubbison, Robert, W.; Meleason, Edward, T.; and Johnson, David, F.: Performance Characteristics From Mach 2.58 To 1.98 of an Axisymmetric Mixed-Compression Inlet System With 60-Percent Internal Contraction. NASA TM X–1739, 1969.
3. Wasserbauer, Joseph, F.; and Choby, David, A.: Mach 2.5 Performance of a Bicone Inlet With Internal Focused Compression and 40-Percent Internal Contraction. NASA TM X–2294, 1971.

4. Wasserbauer, Joseph, F.; Shaw, Robert, J.; and Neumann, Harvey, E.: Design of a Very-Low-Bleed Mach 2.5 Mixed-Compression Inlet With 45 Percent Internal Contraction. NASA TM X–3135, 1975.
5. Baumbick, Robert, J.; Neiner, George, H.; and Cole, Gary, L.: Experimental Dynamic Response of a Two-Dimensional, Mach 2.7, Mixed-Compression Inlet. NASA TN D–6957, 1972.
6. Cole, Gary, L.; Neiner, George, H.; and Baumbick, Robert, J.: Terminal Shock Position and Restart Control of a Mach 2.7, Two-Dimensional, Twin-Duct Mixed-Compression Inlet. NASA TM X–2818, 1973.
7. Anderson, Bernhard, H.: Design of Supersonic Inlets by a Computer Program Incorporating The Method of Characteristics. NASA TN D–4960, 1969.

TABLE I.—INLET GEOMETRY (CENTERLINE)

(a) Centerbody coordinates (design position)

Nondimensional axial coordinate, x/h_c	Nondimensional vertical coordinate, y/h_c	Angle reference, deg
Initial wedge		
0.0000	0.0000	5
Flexible ramp		
0.3883	0.334	5
.5092	.0457	6.011
.6236	.0587	7.038
.7322	.0731	8.080
.8348	.0886	9.138
.9320	.1052	10.212
.9786	.1138	10.755
1.0679	.1317	11.852
1.1523	.1502	12.965
1.2321	.1694	14.093
1.3074	.1891	15.236
1.3434	.1991	15.813
Straight ramp		
1.3434	0.1991	15.813
Aft ramp		
2.9458	0.6529	Hinge point
2.9534	.6536	----------
3.0034	.6573	----------
3.0534	.6598	----------
3.1034	.6611	----------
3.1534	.6611	----------
3.2034	.6598	----------
3.2534	.6573	----------
3.3034	.6536	----------
3.3493	.6492	----------
3.3971	.6440	----------
3.4450	.6396	----------
3.4928	.6346	----------
3.5407	.6293	----------
3.5885	.6238	----------
Aft ramp		
3.6364	0.6182	----------
3.6842	.6121	----------
3.7321	.6053	----------
3.7799	.5984	----------
3.8278	.5909	----------
3.8756	.5828	----------
3.9234	.5743	----------
3.9713	.5656	----------
4.0191	.5566	----------
4.0670	.5467	----------
4.1148	.5368	----------
4.2105	.5166	----------
4.3062	.4952	----------
4.4019	.4737	Hinge point
4.4976	.4512	----------
4.5933	.4280	----------
4.6890	.4049	----------
4.7847	.3809	----------
4.8804	.3569	----------
4.9761	.3325	----------
5.0718	.3085	----------
5.1675	.2823	----------
5.2632	.2567	----------
Straight ramp		
5.3589	0.2308	----------
6.0287	.0479	----------
6.1244	.0325	----------
6.2201	.0211	----------
6.3158	.0163	----------
6.4115	.0134	----------
6.5072	.0115	----------
6.6029	.0101	----------
6.6986	.0091	----------
6.7943	.0086	----------
6.8421	.0086	----------

TABLE I.—Concluded.

(b) Internal cowl coordinates

Nondimensional axial coordinate, x/h_c	Nondimensional vertical coordinate, y/h_c	Angle reference, deg	Nondimensional axial coordinate, x/h_c	Nondimensional vertical coordinate, y/h_c	Angle reference, deg
2.1440	1.0000	5	4.5933	0.8971	----------
2.3705	1.0191	5	4.6890	.8927	----------
2.4739	1.0268	----------	4.7847	.8893	----------
2.5746	1.0316	----------	4.8804	.8863	----------
2.6730	1.0344	----------	4.9761	.8839	----------
2.7693	1.0344	----------	5.0718	.8821	----------
2.8637	1.0316	----------	5.1675	.8810	----------
2.9568	1.0268	----------	5.2631	.8804	----------
3.0489	1.0191	----------	5.3589	.8804	----------
Straight segment			Bypass opening		
3.0622	1.0182	----------	5.4546	0.8804	----------
3.5407	.9751	----------	6.0526	.7847	----------
3.6364	0.9665	----------	6.1244	0.7828	----------
3.7321	.9589	----------	6.2201	.7790	----------
3.8278	.9516	----------	6.3158	.7761	----------
3.9234	.9440	----------	6.4115	.7723	----------
4.0191	.9364	----------	6.5072	.7703	----------
4.1148	.9287	----------	6.6029	.7694	----------
4.2105	.9211	----------	6.6986	.7689	----------
4.3062	.9141	----------	6.7943	.7689	----------
4.4019	.9078	----------	6.8421	.7689	----------
4.4976	.9021	----------			

TABLE II.—LOCATION OF STATIC PRESSURE TAPS ON COWL AND RAMP SURFACES

Ramp		Cowl	
Top	Bottom	Top	Bottom
Nondimensional axial coordinate, x/h_c			
2.7233	2.7233	2.6278	2.6278
2.9145	.9145	.8667	.8667
2.9623	.9623	3.0100	.0100
3.0100	3.0100	.1056	.1056
.0578	.0578	.2011	.2011
.1056	.1056	.2489	.2489
.1534	.1534	.2967	.2967
.2011	--------	.3444	.3444
.2489	--------	.3922	.3922
.2967	--------	.4400	.4400
.3445	--------	.4878	.4878
.3923	--------	.5356	.5356
.4400	--------	.5833	.5833
.4878	--------	.6311	.6311
.5356	--------	.7745	.7745
.5834	--------	.9234	.8756
.6799	--------	4.4976	4.4976
.7754	--------	5.1675	5.1196
.8710	.8710	6.3541	6.3541
4.2584	--------	--------	--------
.7368	--------	--------	--------
5.1196	5.1196	--------	--------
.4545	--------	--------	--------
.8373	--------	--------	--------
6.3541	6.3541	--------	--------

TABLE III.—TRANSVERSE COWL COORDINATES FOR SUBSONIC DIFFUSER

[Tolerance, ±0.005 in.]

Model station	Distance from model centerline, in.		Model station	Distance from model centerline, in.		Model station	Distance from model centerline, in.		Model station	Distance from model centerline, in.	
	Spanwise, z	Vertical, y		Spanwise, z	Vertical, y		Spanwise, z	Vertical, y		Spanwise, z	Vertical, y
66.767	0.000	10.083	71.5	0.000	9.705	76.5	0.000	9.375	81.5	0.000	9.218
	2.000			2.000	9.667		2.000	9.287		2.000	9.074
	4.000			4.000	9.544		4.000	9.004		4.000	8.614
	5.000			5.000	9.442		5.000	8.769		5.000	8.233
	6.000			6.000	9.301		6.000	8.444		6.000	7.706
	7.000			7.000	9.097		7.000	7.974		7.000	6.942
	7.500			7.500	8.950		7.500	7.634		7.500	6.388
	8.000			8.000	8.715		8.000	7.094		8.000	5.511
	8.200	10.083		8.200	8.437		8.200	6.452		8.200	4.468
67.5	0.000	10.024	72.5	0.000	9.625	77.5	0.000	9.329	82.5	0.000	9.206
	2.000			2.000	9.577		2.000	9.230		2.000	9.051
	4.000			4.000	9.424		4.000	8.913		4.000	8.554
	5.000			5.000	9.296		5.000	8.650		5.000	8.141
	6.000			6.000	9.120		6.000	8.287		6.000	7.571
	7.000			7.000	8.866		7.000	7.761		7.000	6.746
	7.500			7.500	8.681		7.500	7.379		7.500	6.148
	8.000			8.000	8.388		8.000	6.774		8.000	5.199
	8.200	10.024		8.200	8.040		8.200	6.056		8.200	4.072
68.5	0.000	9.944	73.5	0.000	9.552	78.5	0.000	9.293	83.5	0.000	9.200
	2.000	9.934		2.000	9.454		2.000	9.183		2.000	9.033
	4.000	9.904		4.000	9.309		4.000	8.831		4.000	8.498
	5.000	9.878		5.000	9.156		5.000	8.539		5.000	8.054
	6.000	9.843		6.000	8.944		6.000	8.136		6.000	7.441
	7.000	9.792		7.000	8.637		7.000	7.552		7.000	6.553
	7.500	9.755		7.500	8.415		7.500	7.128		7.500	5.909
	8.000	9.697		8.000	8.062		8.000	6.457		8.000	4.888
	8.200	9.627		8.200	7.643		8.200	5.659		8.200	3.675
69.5	0.000	9.865	74.5	0.000	9.486	79.5	0.000	9.262	84.5	0.000	9.200
	2.000	9.846		2.000	9.418		2.000	9.141		2.000	9.021
	4.000	9.784		4.000	9.201		4.000	8.754		4.000	8.448
	5.000	9.733		5.000	9.021		5.000	8.432		5.000	7.972
	6.000	9.663		6.000	8.773		6.000	7.988		6.000	7.314
	7.000	9.561		7.000	8.413		7.000	7.345		7.000	6.362
	7.500	9.487		7.500	8.152		7.500	6.879		7.500	5.672
	8.000	9.369		8.000	7.788		8.000	6.140		8.000	4.578
	8.200	9.230		8.200	7.246		8.200	5.262		8.200	3.278
70.5	0.000	9.785	75.5	0.000	9.427	80.5	0.000	9.237	84.88	0.000	9.200
	2.000	9.756		2.000	9.349		2.000	9.105		2.000	9.017
	4.000	9.664		4.000	9.099		4.000	8.681		4.000	8.428
	5.000	9.588		5.000	8.892		5.000	8.330		5.000	7.940
	6.000	9.482		6.000	8.606		6.000	7.845		6.000	7.266
	7.000	9.329		7.000	8.192		7.000	7.142		7.000	6.290
	7.500	9.218		7.500	7.891		7.500	6.633		7.500	5.582
	8.000	9.043		8.000	7.415		8.000	5.325		8.000	4.460
	8.200	8.834		8.200	6.849		8.200	4.865		8.200	3.127

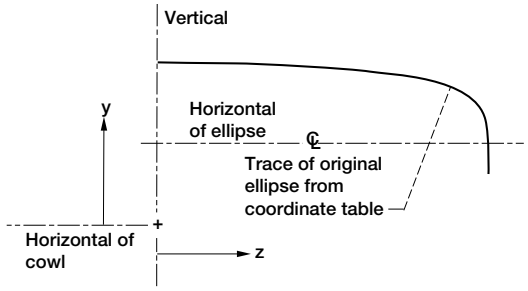

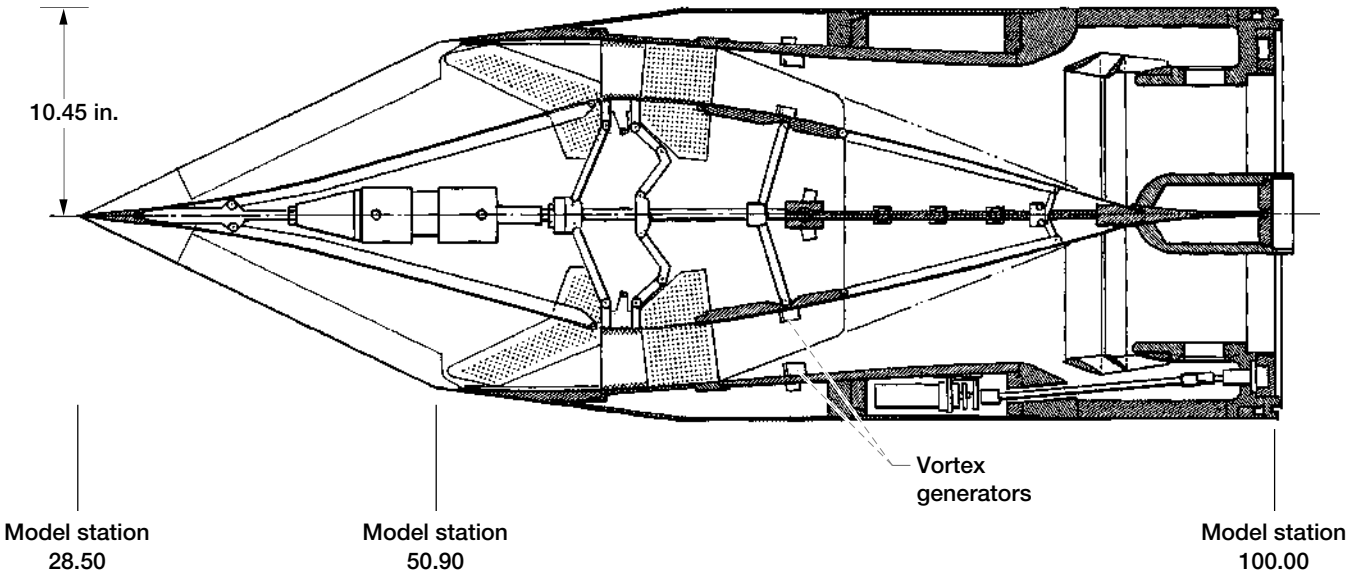

(a)

Figure 1.—Two-dimensional inlet. (a) Inlet cross section. (b) Inlet and cold pipe in test section. (c) Isometric view of two-dimensional inlet. (d) Location of bleed in supersonic diffuser. (e) Vortex generator details. (f) Theoretical shock structure. (g) Theoretical surface static pressure and Mach number distributions.

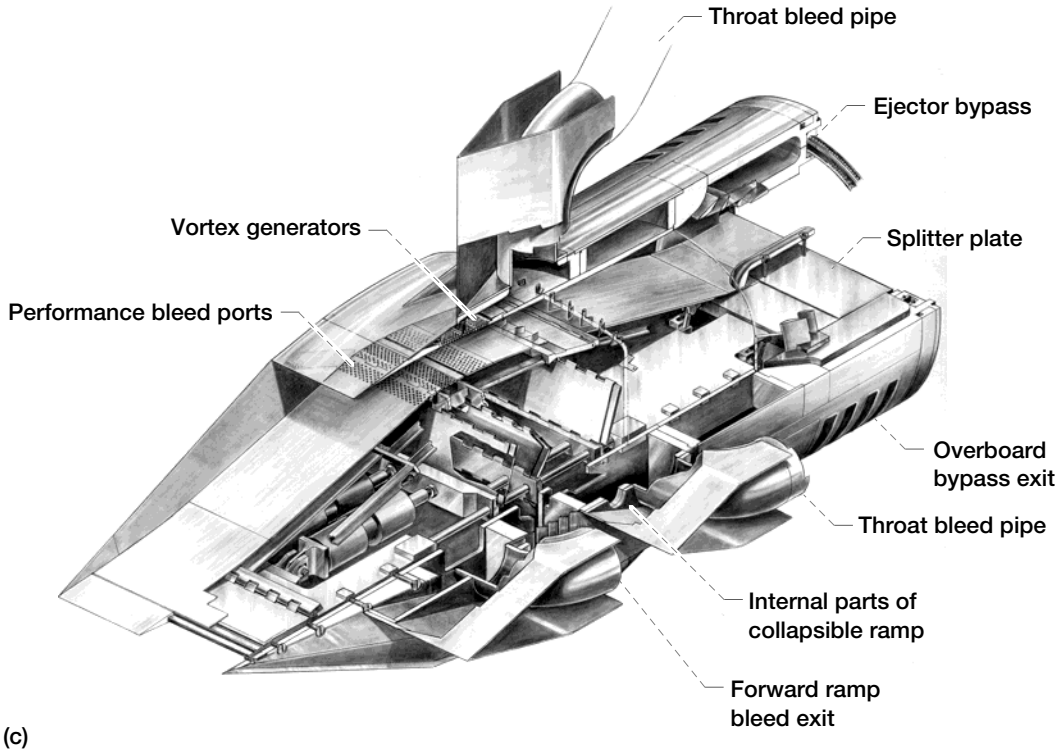

(c)

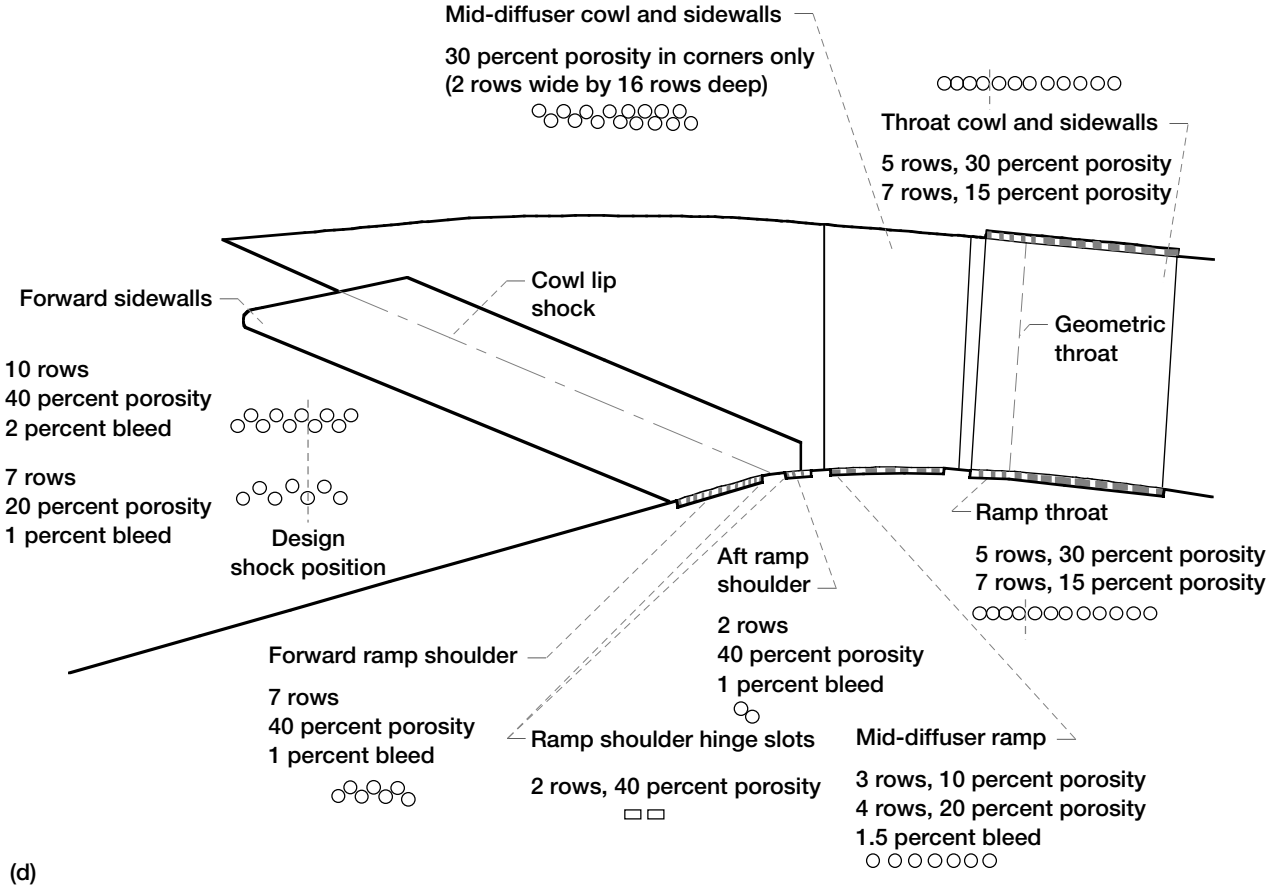

(d)

Figure 1.—Continued. (c) Isometric view of two-dimensional inlet. (d) Bleed patterns in supersonic diffuser.

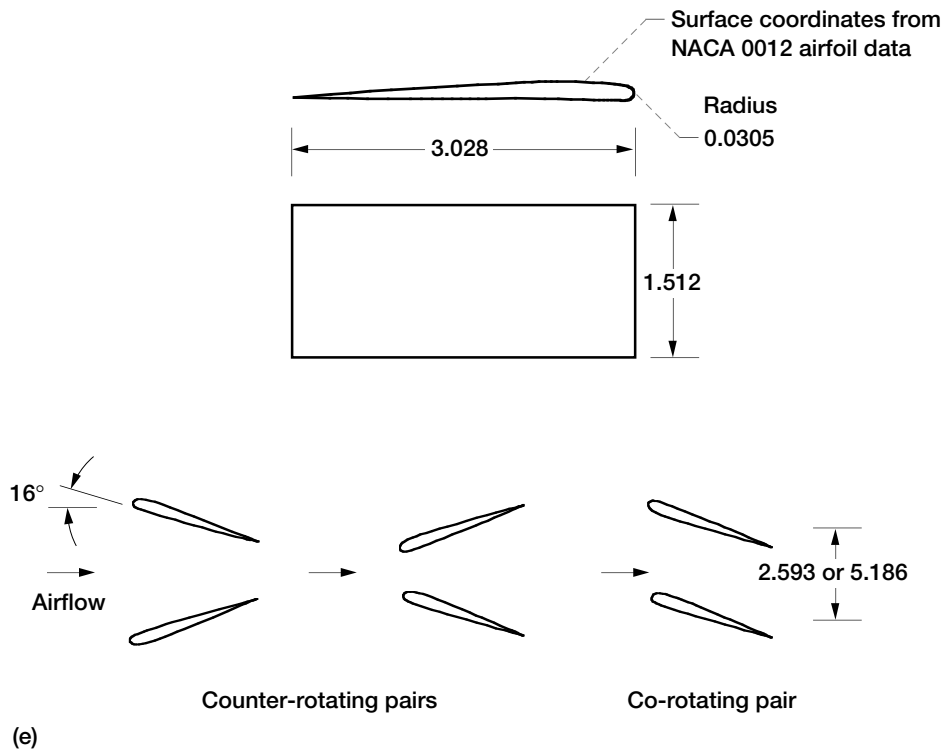

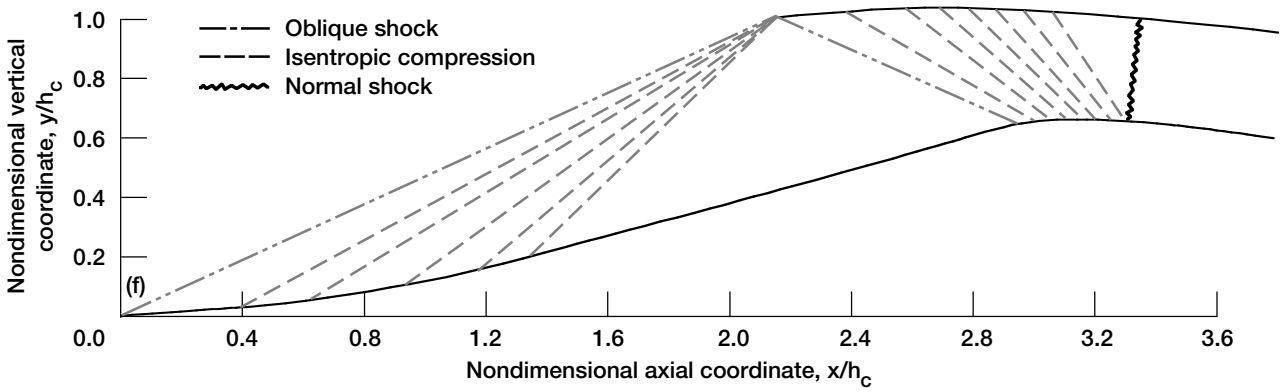

Figure 1.—Continued. (e) Vortex generator details. All dimensions are in centimeters. (f) Theoretical shock structure.

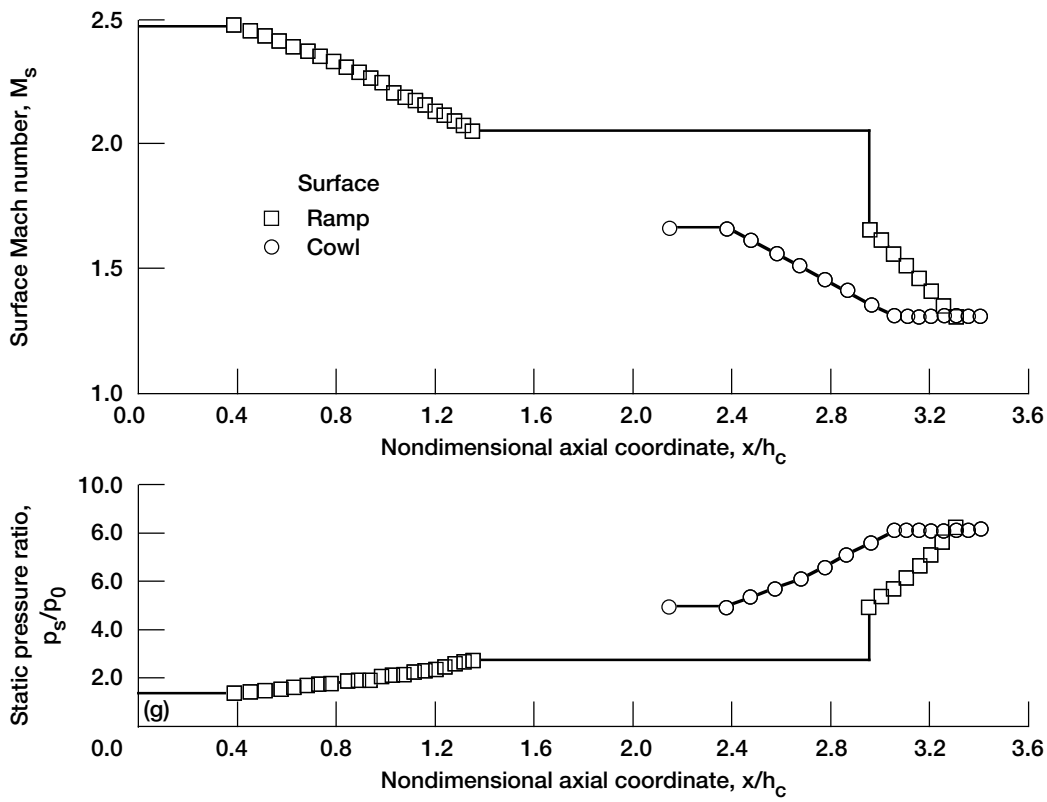

Figure 1.—Concluded. (g) Theoretical surface static pressure and Mach number distributions.

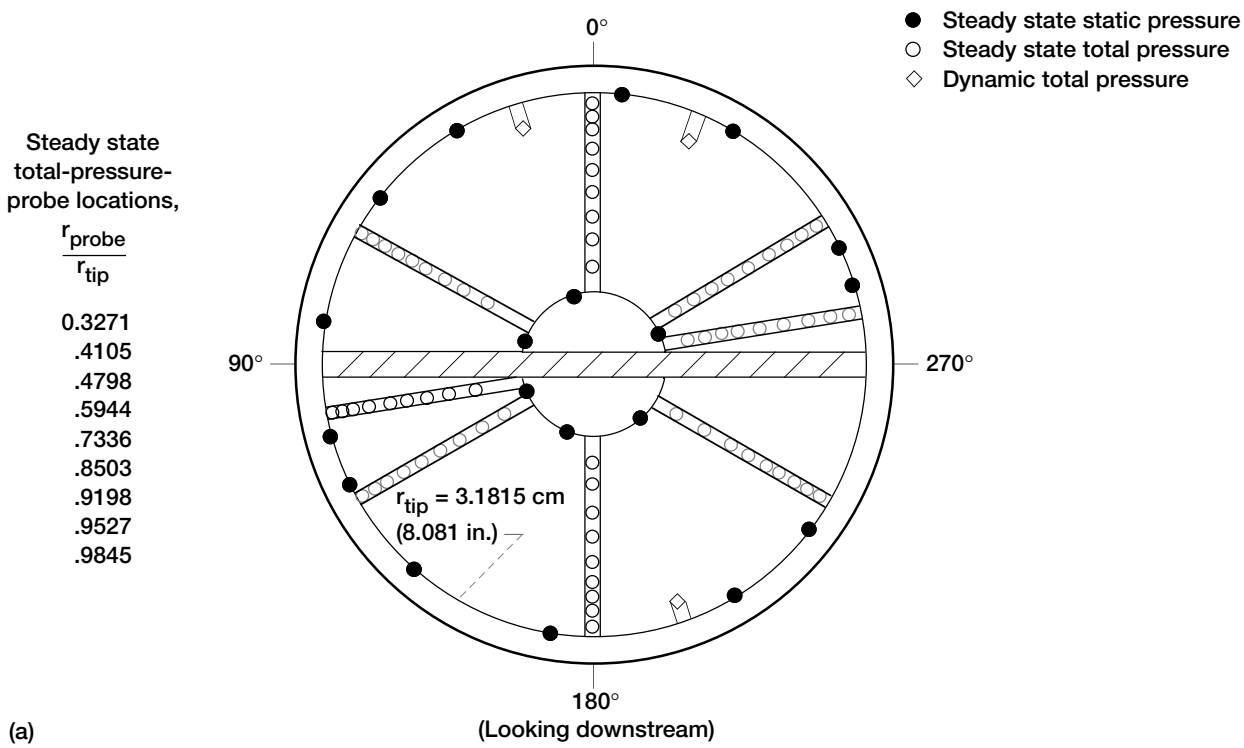

Figure 2.—Instrumentation. (a) Compressor face. (b) Ramp shoulder and sidewall boundary layer rakes. (c) Aft throat corner rakes.

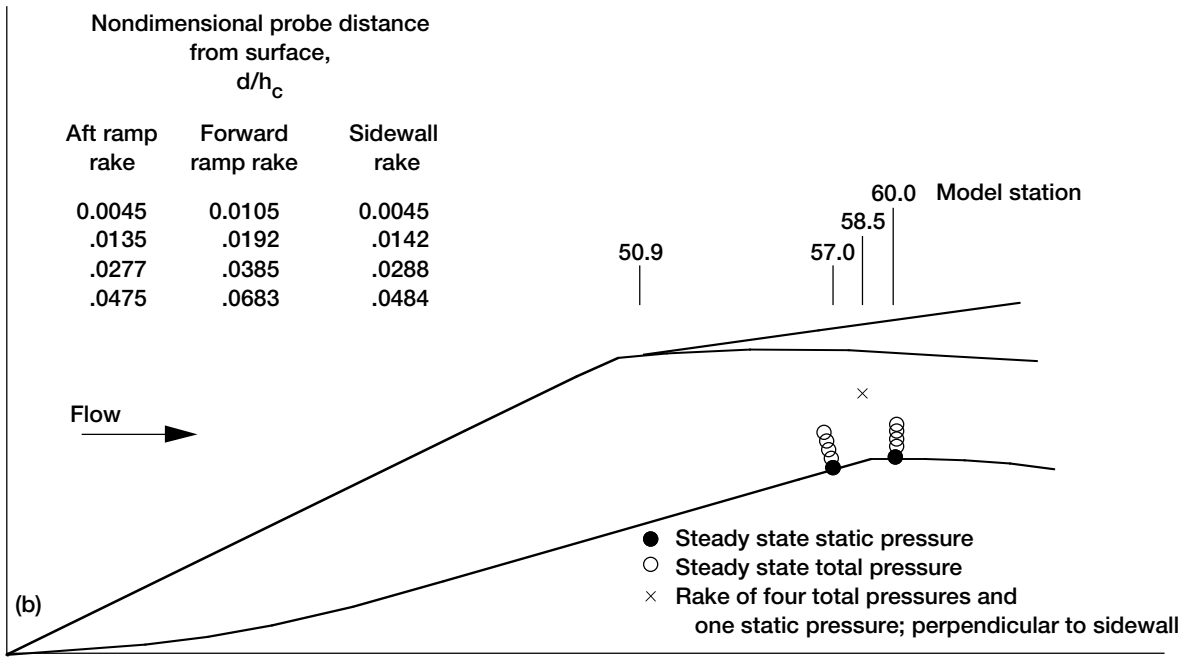

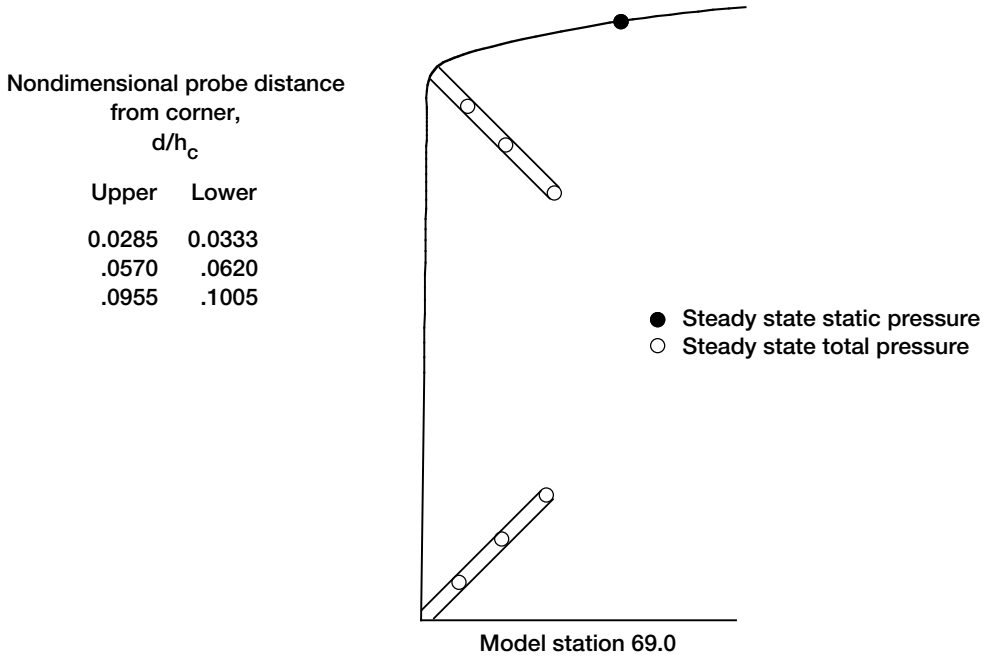

(c)

Figure 2.—Concluded. (b) Ramp shoulder and sidewall boundary layer rakes. (c) Aft throat corner rakes.

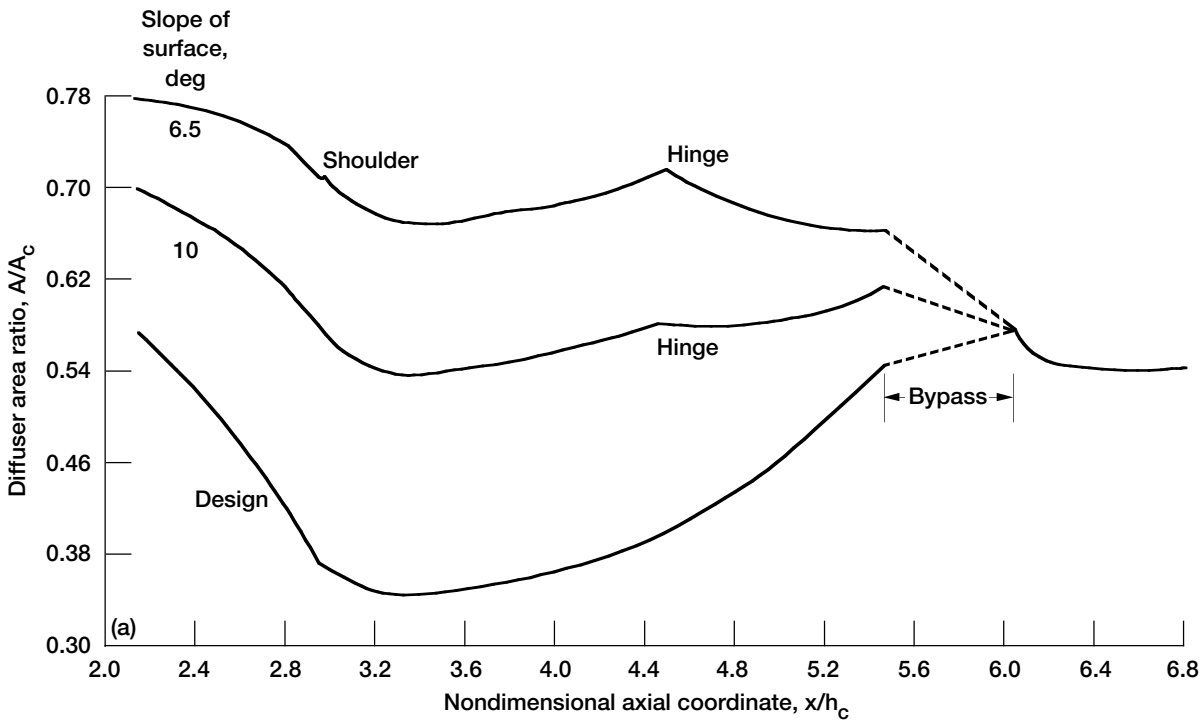

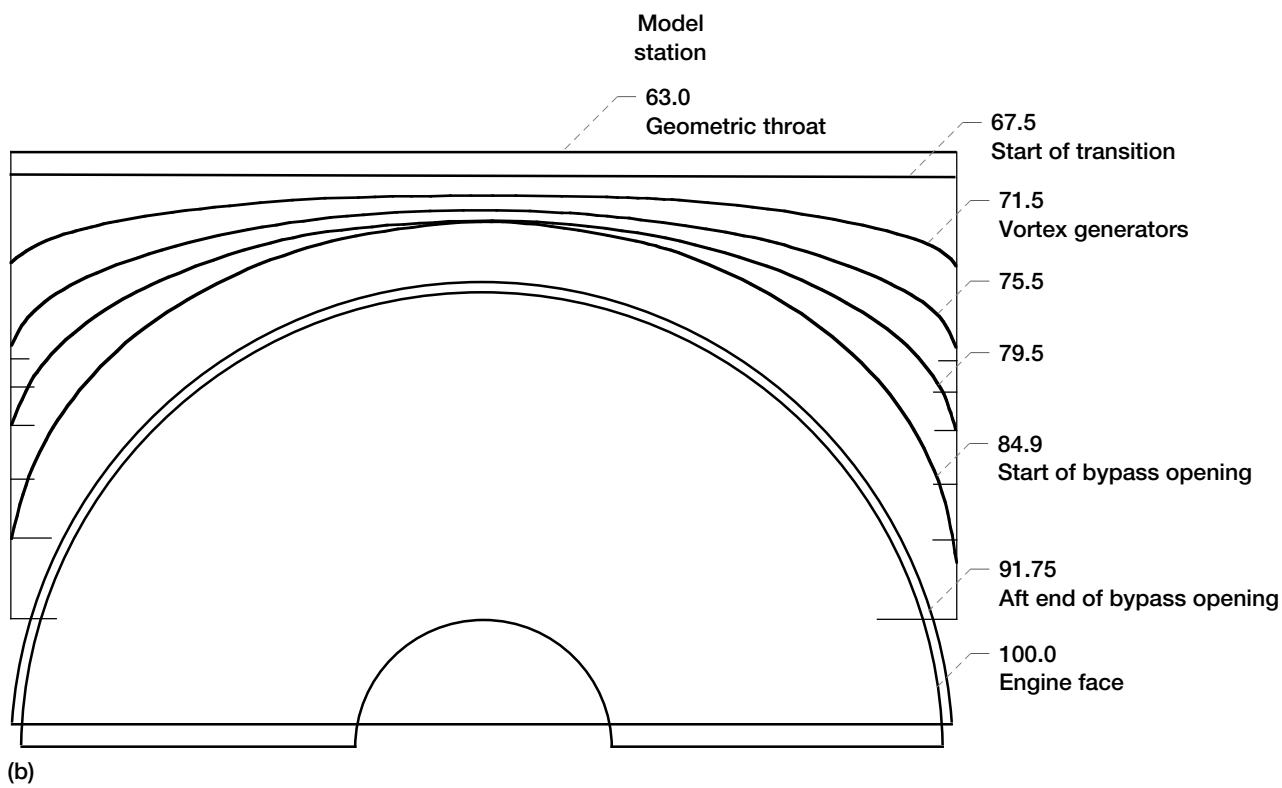

Figure 3.—Inlet geometry. (a) Inlet area variation. (b) Subsonic diffuser geometric variation for 70-30, two-dimensional inlet.

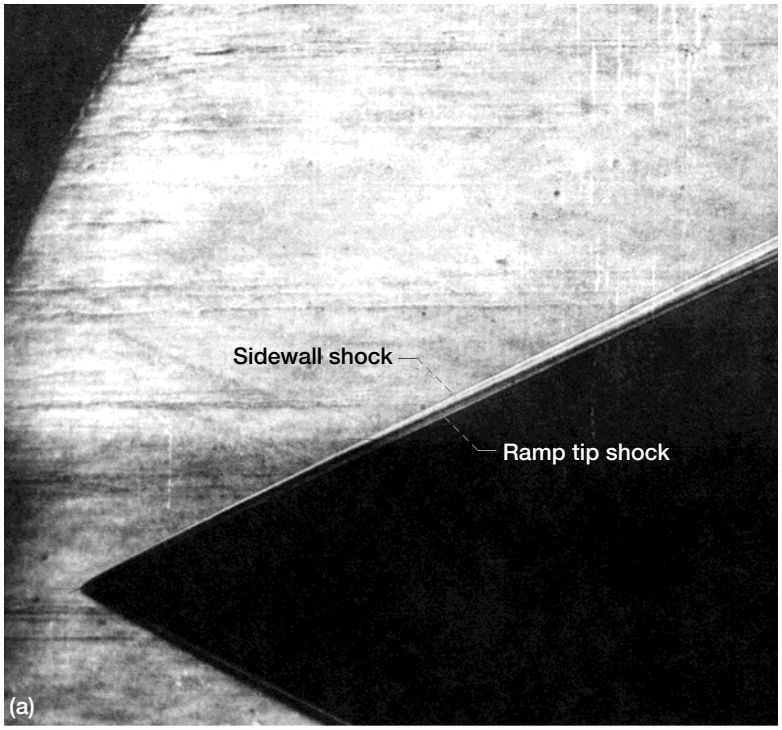

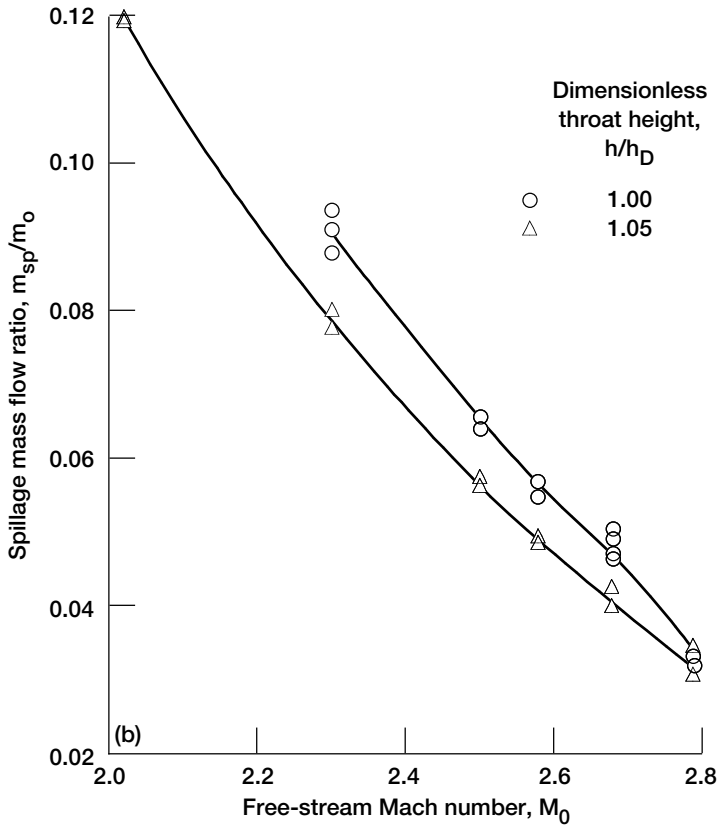

Figure 4.—Inlet spillage. (a) Inlet shock structure. Configuration SS-1; free-stream Mach number M_0 = 2.68; angle of yaw β = 0°; design ramp position δ = 15.81°. (b) Effect of free-stream Mach number on spillage.

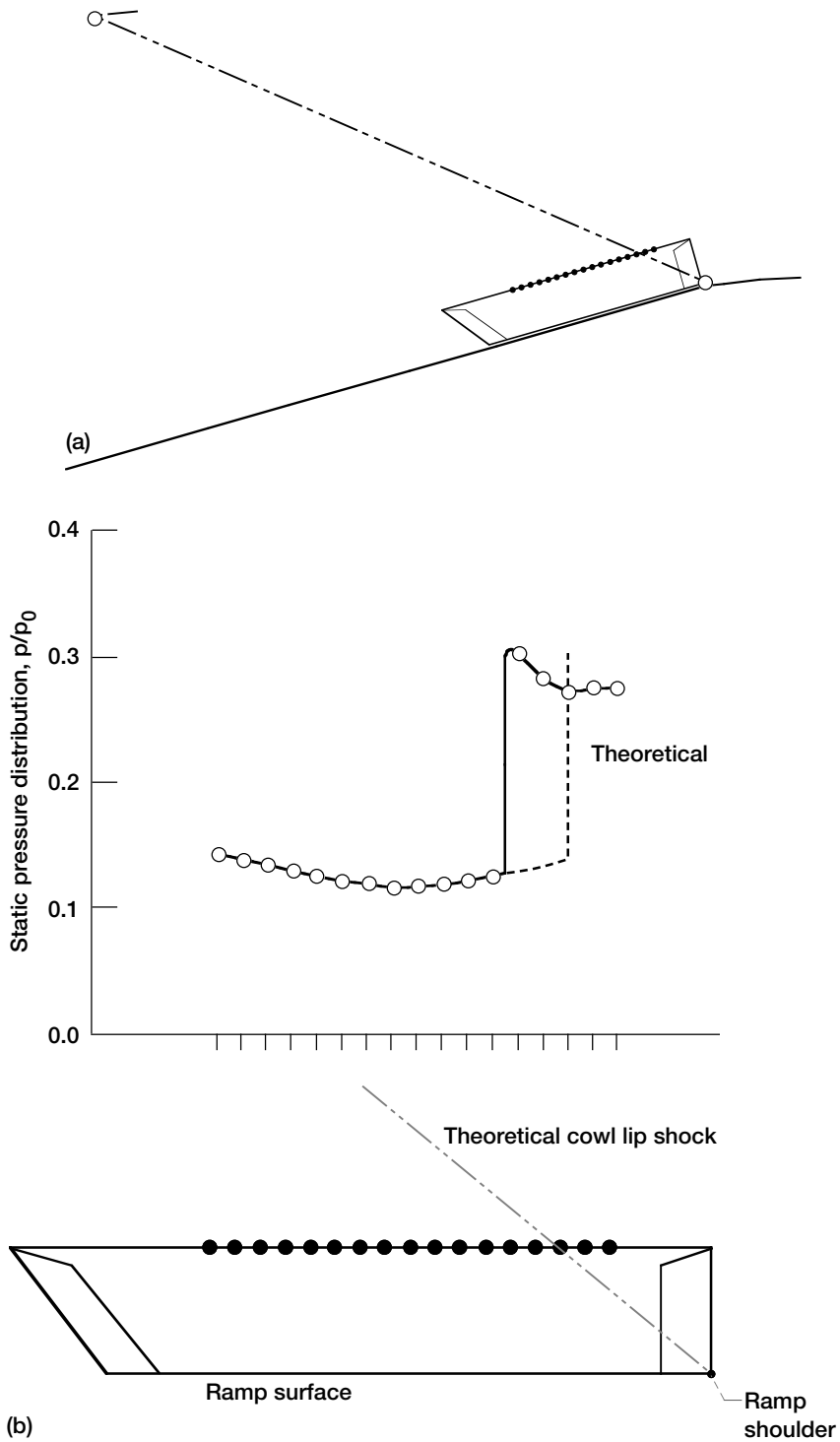

Figure 5.—Cowl shock location. (a) Cowl lip shock position rake. Design ramp position $\delta = 15.81°$. (b) Cowl lip shock rake static pressure profile. Free-stream Mach number $M_0 = 2.68$; design ramp position $\delta = 15.81°$. (c) Location of cowl lip shock impingement on ramp. (d) Variation of inlet total pressure recovery with ramp position and bleed mass flow. Free-stream Mach number $M_0 = 2.68$.

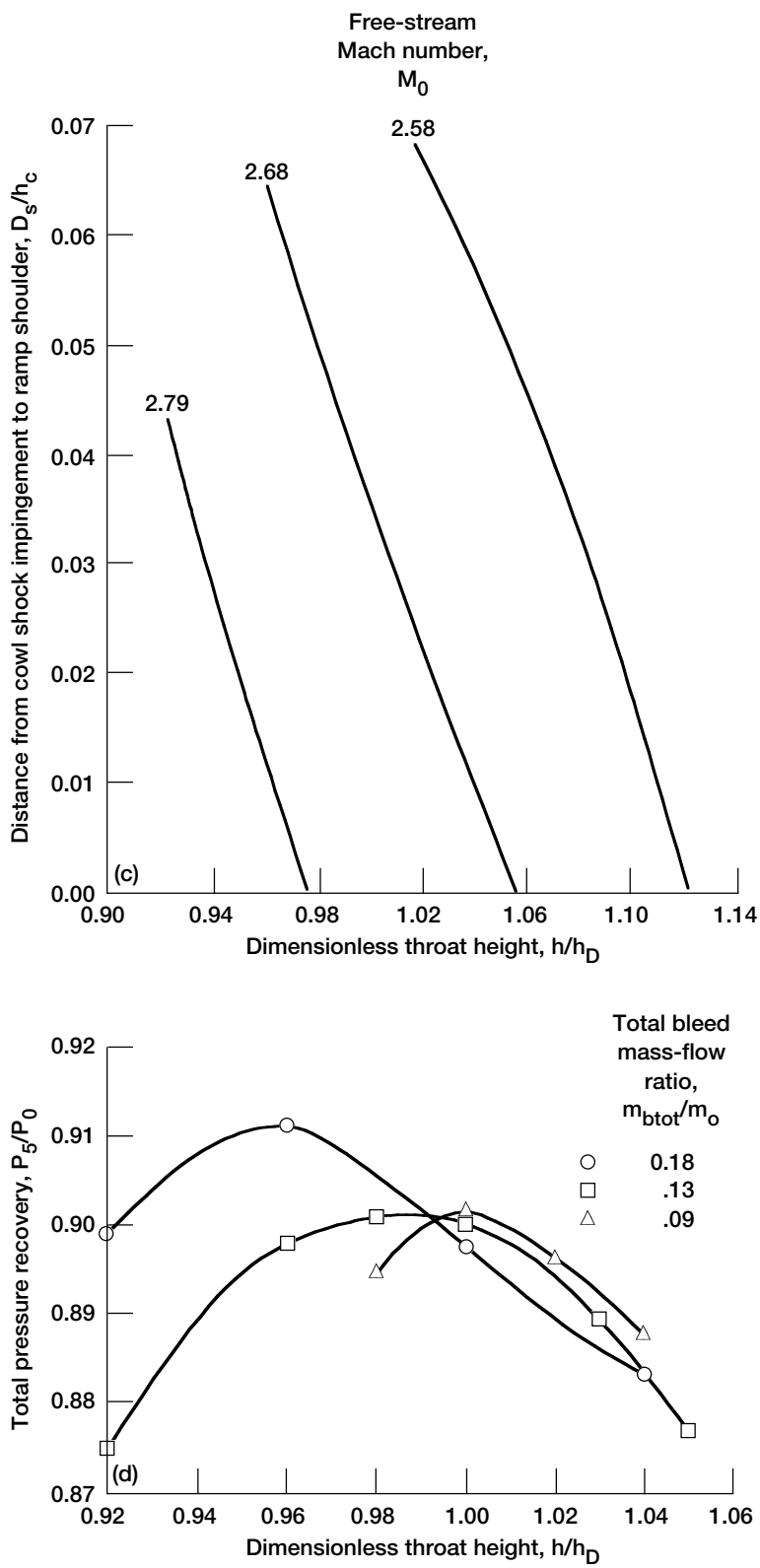

Figure 5.—Concluded. (c) Location of cowl lip shock impingement on ramp. (d) Variation of inlet total pressure recovery with ramp position and bleed mass flow. Free-stream Mach number M_0 = 2.68.

Configuration (change)	Ramp bleed shoulder		Bleed mass-flow ratio, m_b/m_o	Forward sidewall bleed		Bleed mass-flow ratio, m_b/m_o	Supercritical unstart angle, β_{uns}, deg
					Design shock position		
Open bleed	RS-1	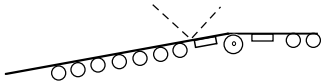	0.016	FS-2	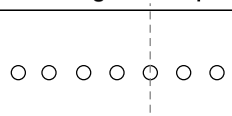	0.014	2.4
Some ramp bleed closed ahead of shock	RS-3	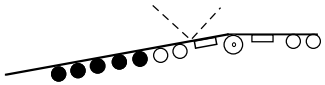	0.016	FS-2	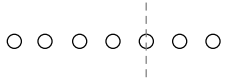	0.014	2.3
Some sidewall bleed closed ahead of shock	RS-3	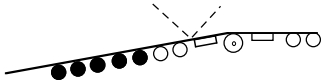	0.016	FS-3	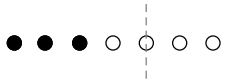	0.013	1.95
Ramp bleed closed behind shock	RS-4	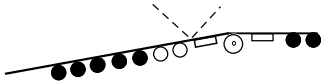	0.013	FS-3	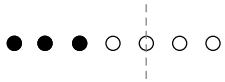	0.013	1.0
Some sidewall bleed closed behind shock	RS-2	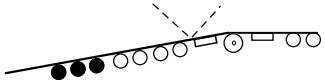	0.016	FS-4	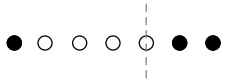	0.010	1.5

(a)

Figure 6.—Effect of bleed variations in vicinity of cowl lip shock on yaw angle tolerance. (a) Summary of bleed patterns. (b) Effect of bleed variation on sidewall boundary layer with fixed exits. (c) Effect of bleed variation on ramp boundary layer with fixed exits. (d) Comparison of ramp boundary layer profiles before and after ramp shoulder. Bleed configuration RS-2.

	Configuration	Porosity, percent	Bleed mass-flow ratio, $(m_b/m_o)_{forward\ sidewall}$
○	FS-1	40 All holes open	0.021
□	FS-2	20 All holes open	.014
△	FS-3	20 Forward three of seven rows closed	.013
◇	FS-4	20 First row plus aft two rows closed	.010

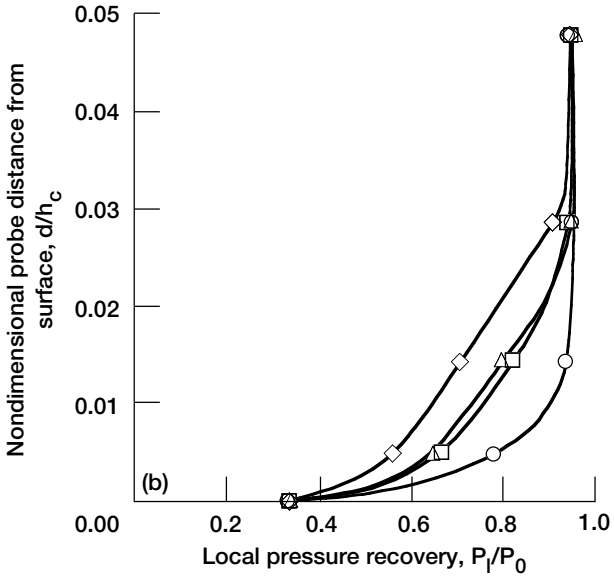

		Configuration	Bleed plenum pressure ratio, P_{pl}/P_0	Bleed mass-flow ratio, $(m_b/m_o)_{ramp\ shoulder}$
○	All ramp shoulder bleed open, one exit	RS-1	0.143	0.0165
□	Front three rows closed, one exit	RS-2	.143	.0161
△	Front five rows closed, one exit	RS-3	.137	.0159
◇	Front five rows plus aft two rows closed, one exit	RS-4	.113	.0130

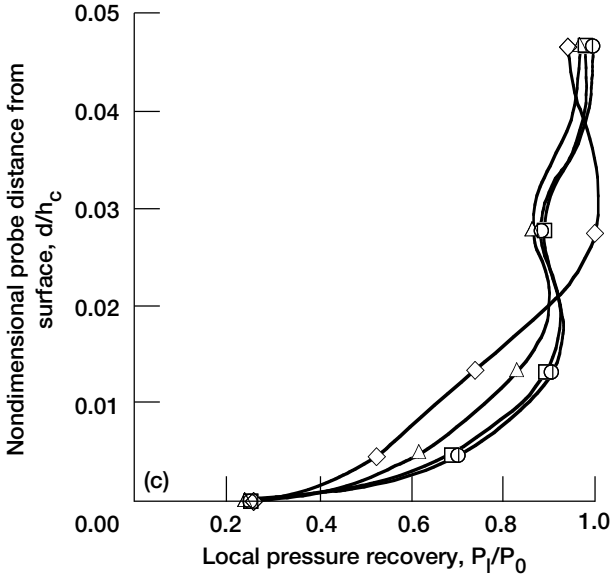

Figure 6.—Continued. (b) Effect of bleed variation on sidewall boundary layer with fixed exits. (c) Effect of bleed variation on ramp boundary layer with fixed exits. Ramp boundary layer rake 2 (behind ramp shoulder at model station 60.0).

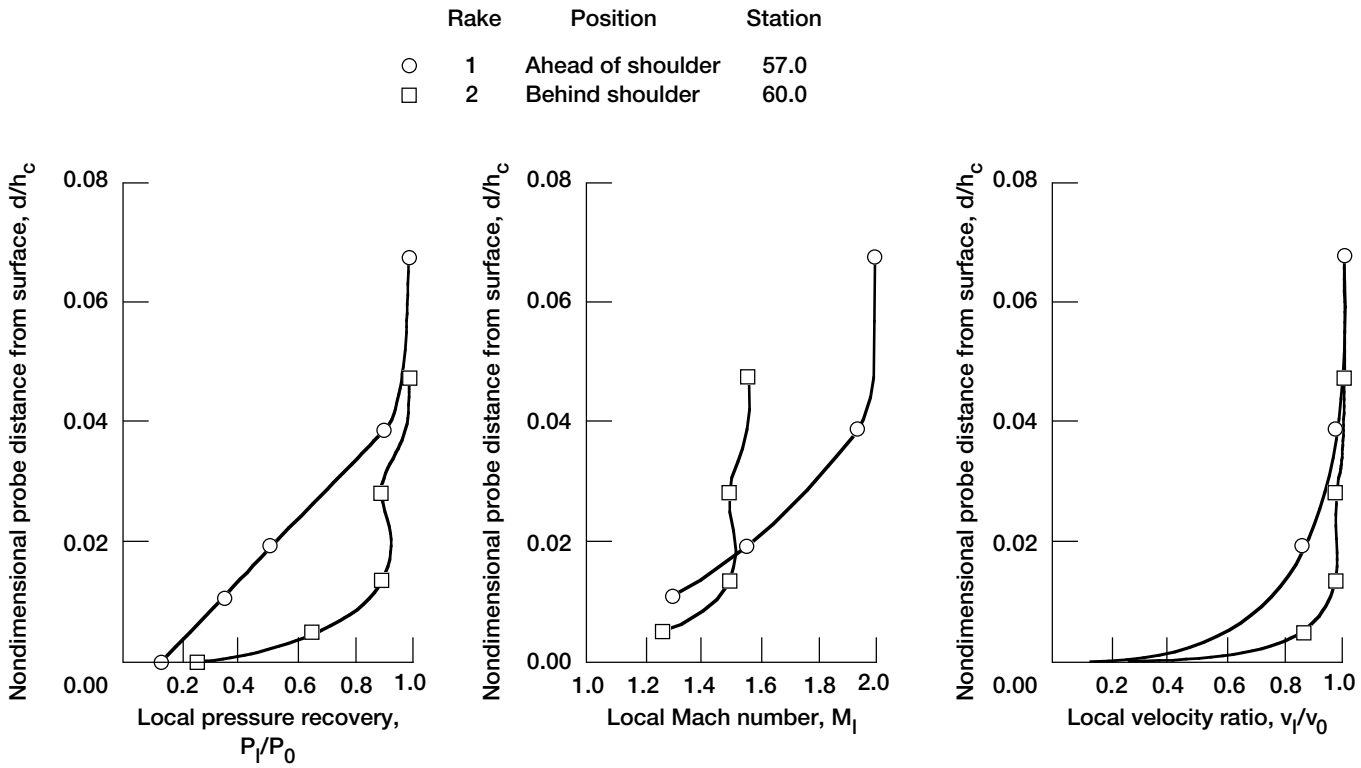

Figure 6.—Concluded. (d) Comparison of ramp boundary layer profiles before and after ramp shoulder. Bleed configuration RS-2.

Configuration (change)	Forward Sidewall bleed		Bleed mass-flow ratio, m_b/m_o	Mid-diffuser bleed		Bleed mass-flow ratio, m_b/m_o	Supercritical unstart angle, β_{uns}, deg
		Design shock position					
All mid-diffuser bleed closed	FS-1	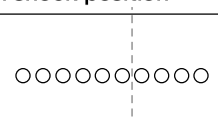	0.021	MD-0	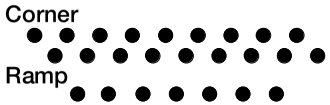	0.000	1.90
Mid-diffuser corner bleed	FS-1		0.021	MD-1	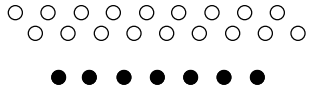	0.007	2.35
All mid-diffuser bleed open	FS-1		0.021	MD-4	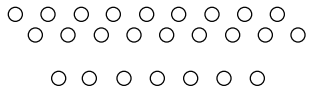	0.013	3.75
Reduced sidewall bleed; all mid-diffuser bleed closed	FS-2	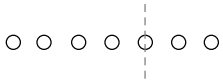	0.014	MD-0	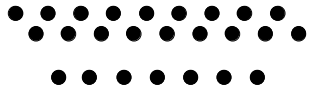	0.000	1.50
Corner bleed plus some ramp bleed	FS-2	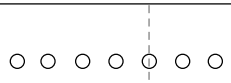	0.013	MD-2	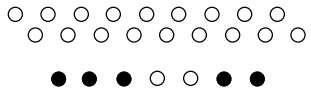	0.010	2.40
Ramp bleed moved aft; some sidewall bleed closed ahead of shock	FS-2	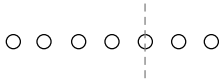	0.013	MD-3	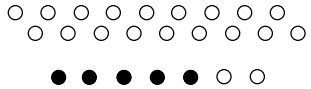	0.010	3.20

Figure 7.—Effect of mid-diffuser bleed variations on yaw angle tolerance.

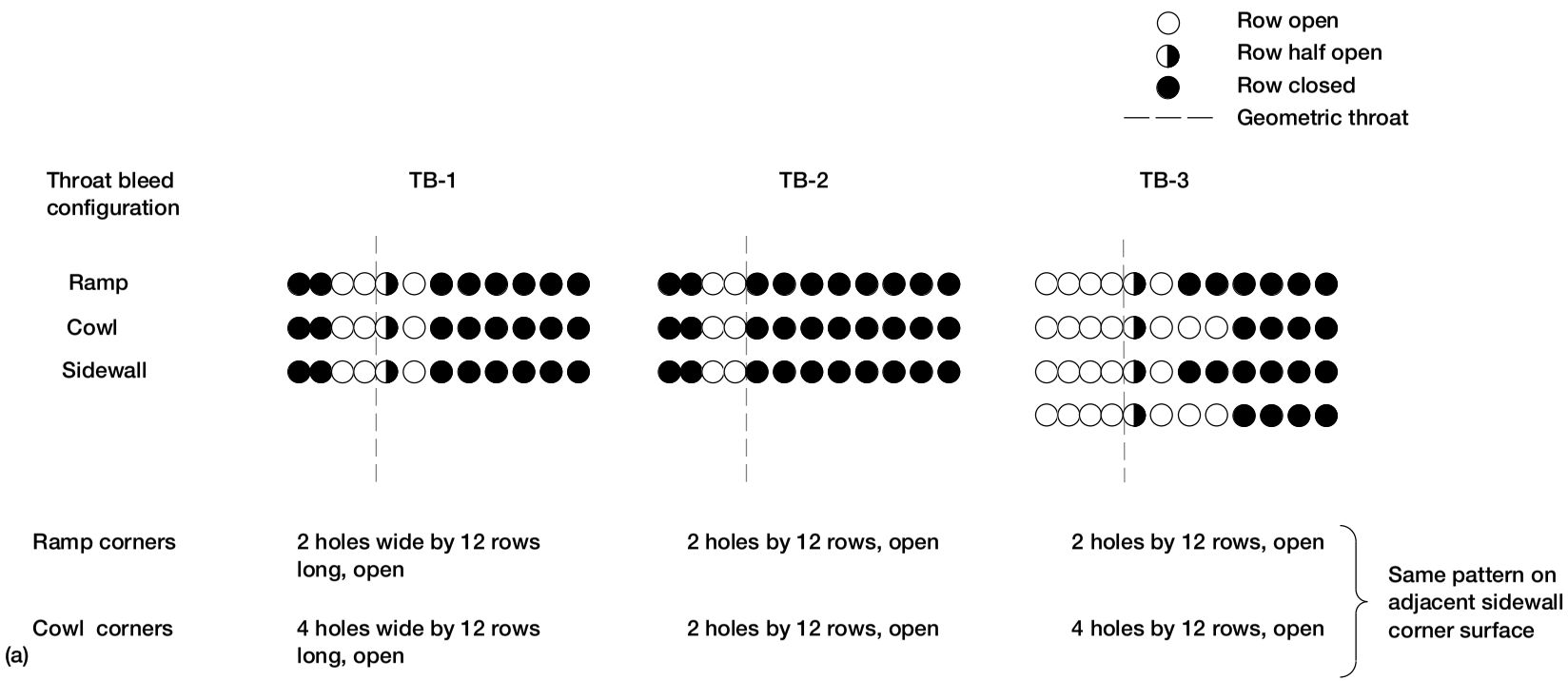

Figure 8.—Effect of throat bleed variation on inlet performance. (a) Throat bleed configurations. (b) Corner throat rake total pressure profiles. Model station 69.0. (c) Inlet total pressure recovery. Free-stream Mach number $M_0 = 2.68$; design ramp position $\delta = 15.81$. (d) Inlet distortion. Free-stream Mach number $M_0 = 2.68$; design ramp position $\delta = 15.81$.

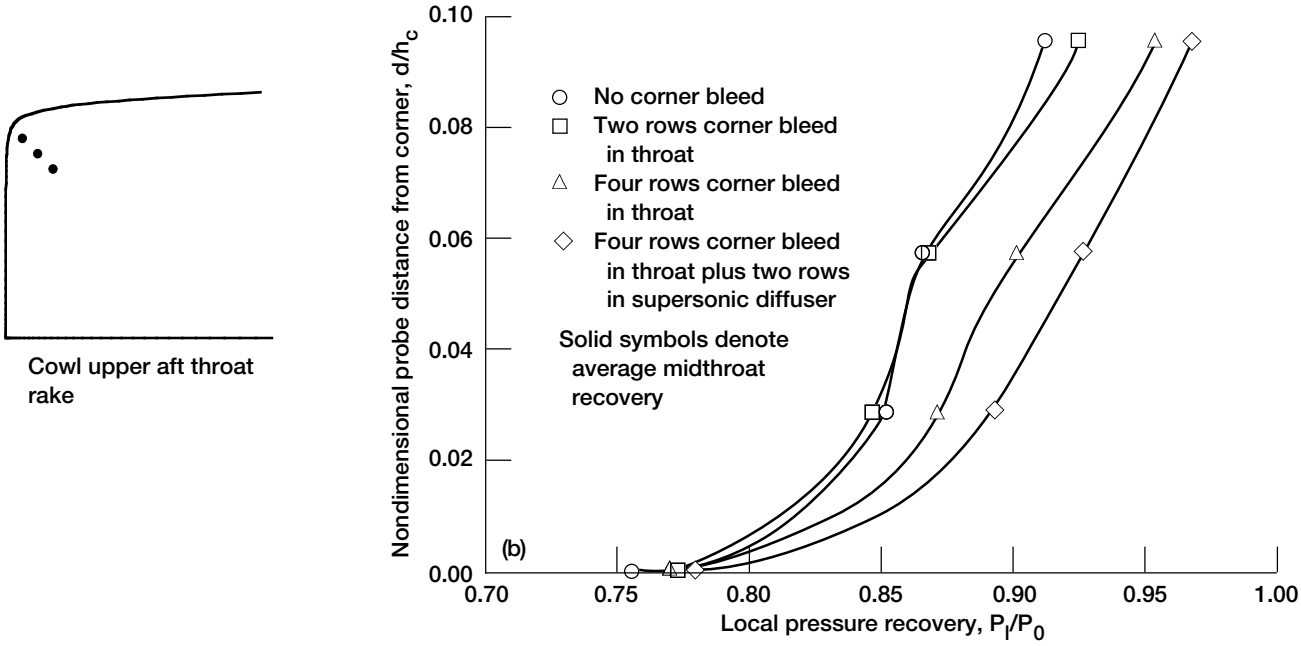

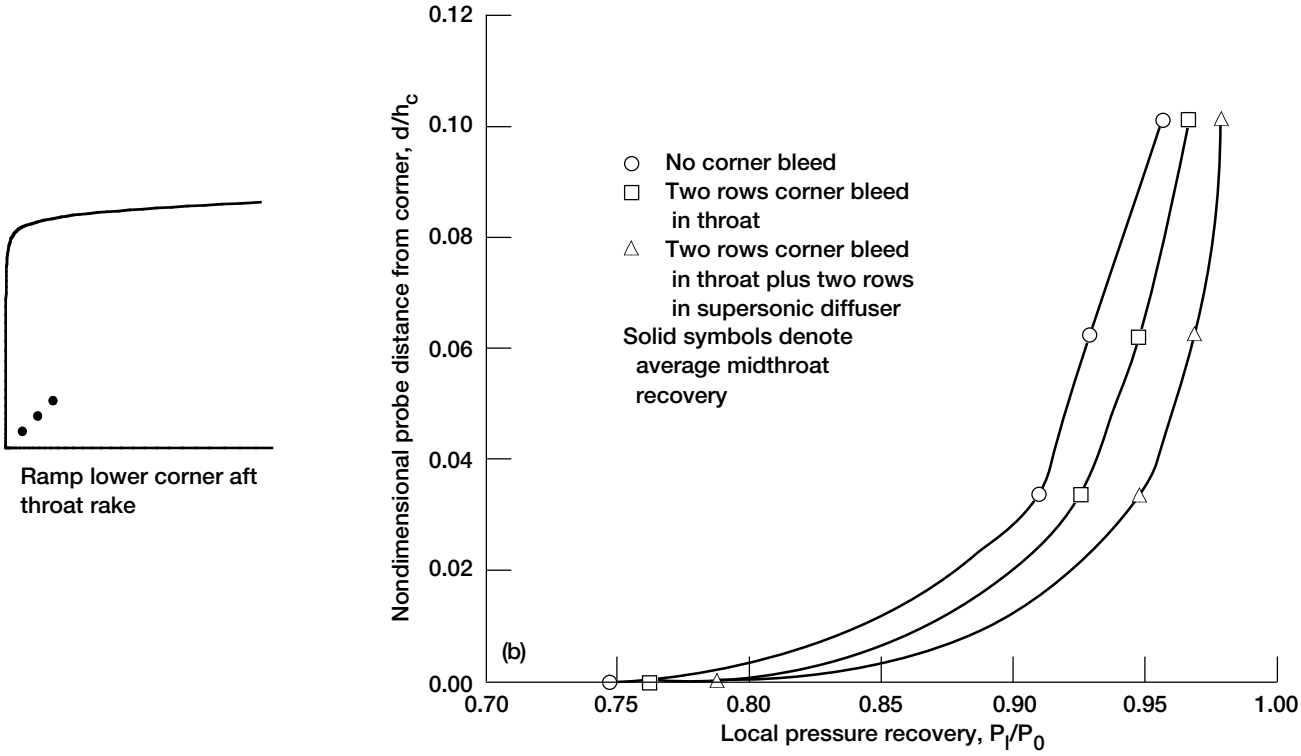

Figure 8.—Continued. (b) Corner throat rake total pressure profiles. Model station 69.0.

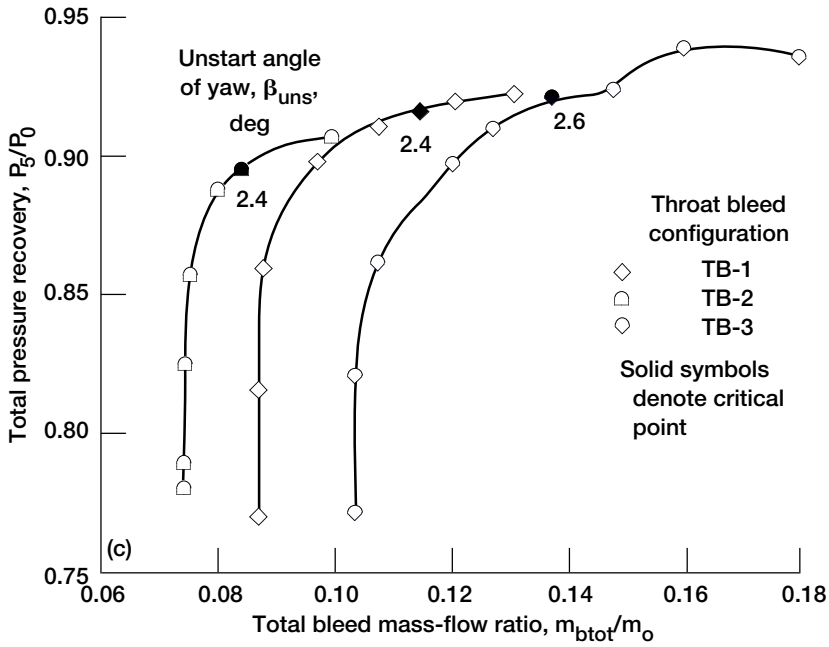

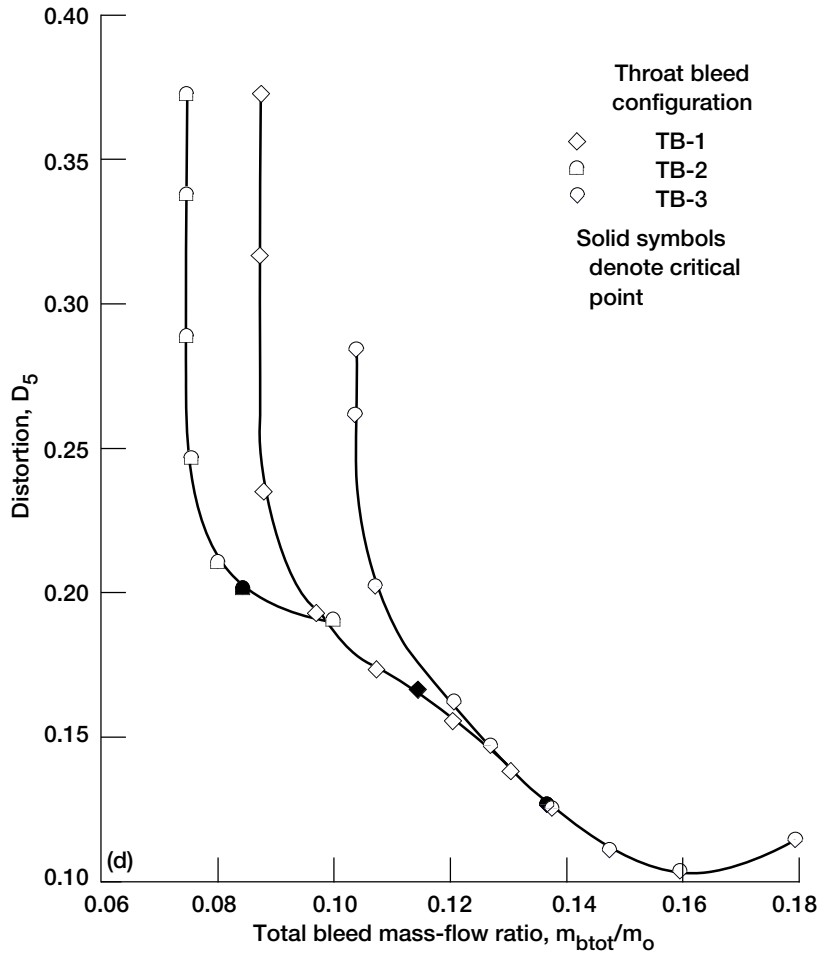

Figure 8.—Concluded. (c) Inlet total pressure recovery. Free-stream Mach number M_0 = 2.68; design ramp position, δ = 15.81. (d) Inlet distortion. Free-stream Mach number M_0 = 2.68; design ramp position δ = 15.81.

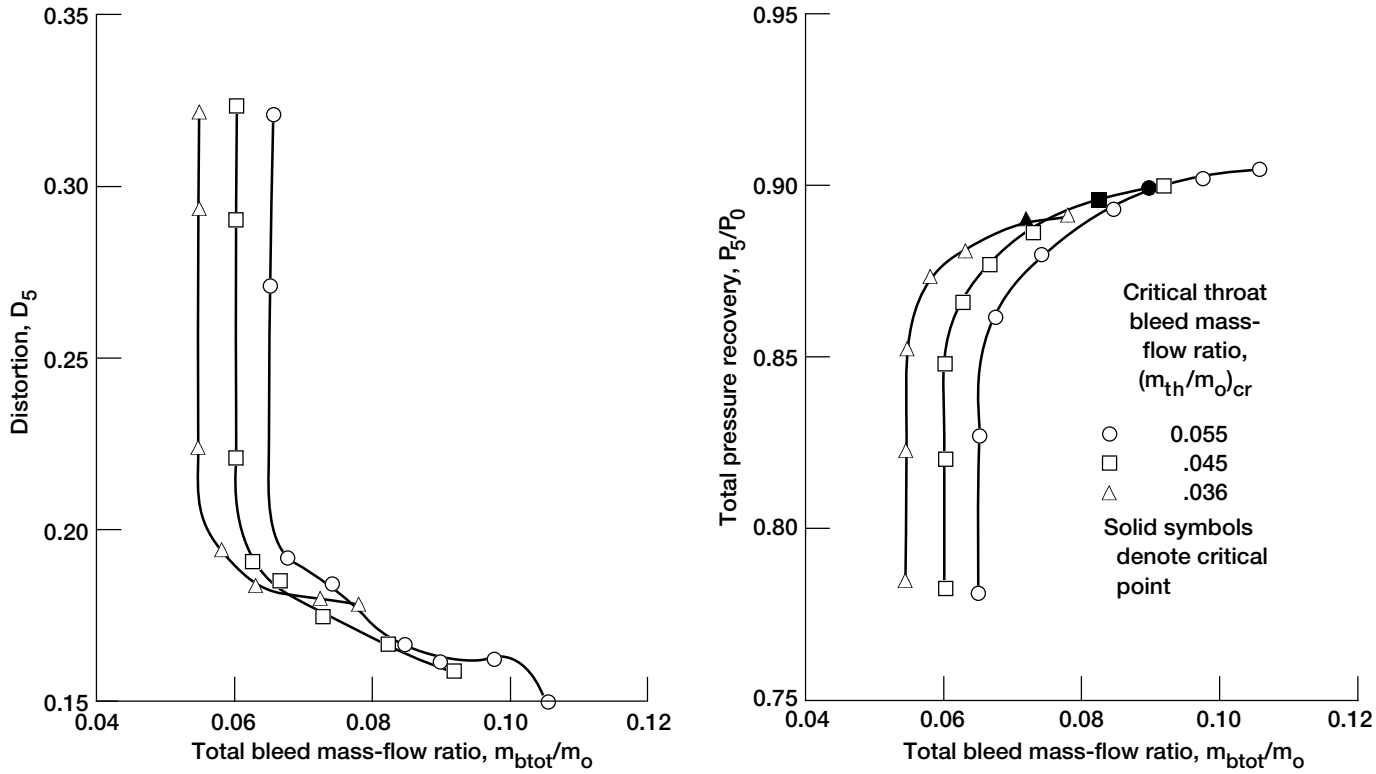

Figure 9.—Performance of selected throat bleed configuration (TB-1) for various amounts of throat bleed mass flow. Free-stream Mach number = 2.68; design ramp position δ = 15.81.

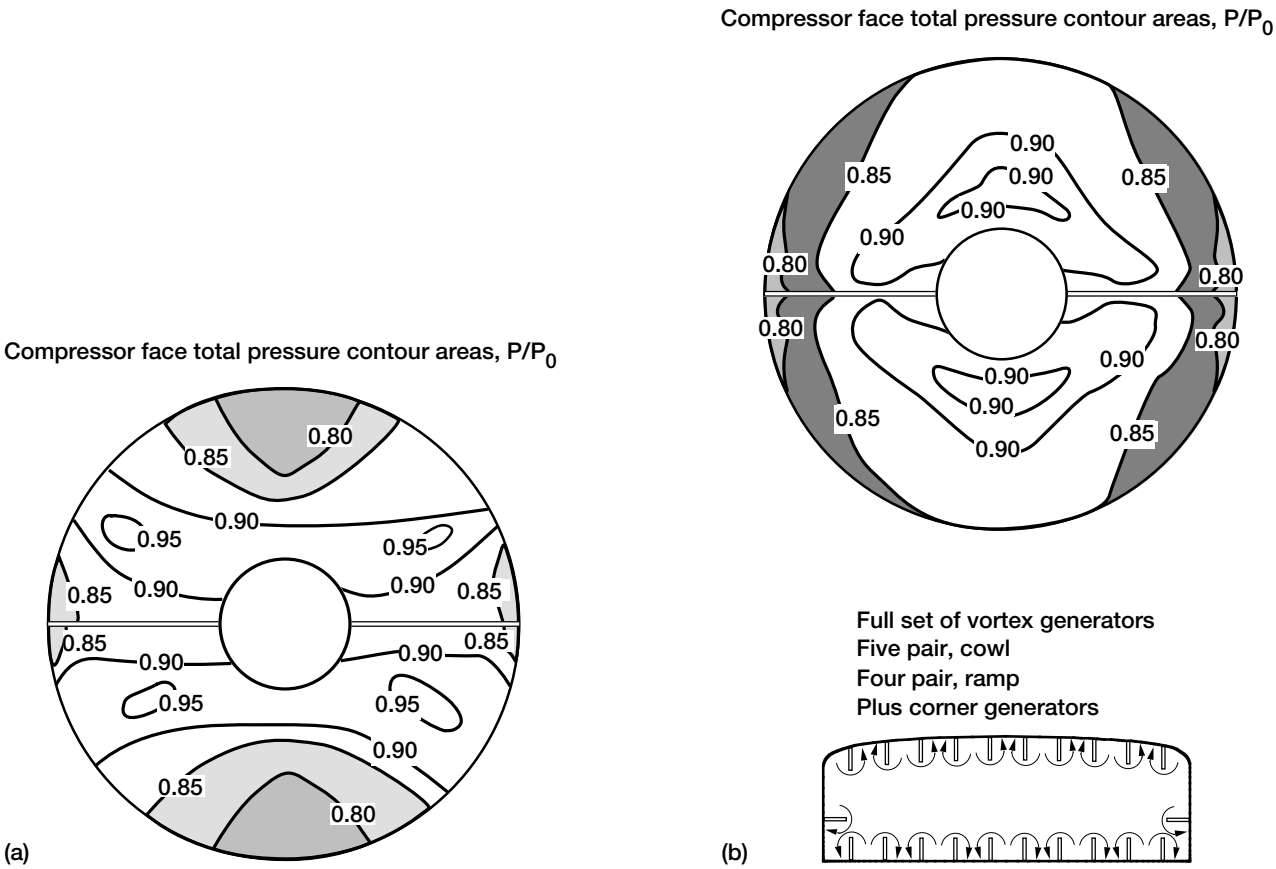

Figure 10.—Effect of vortex generators on compressor face total pressure contours for critical inlet operation. (a) No vortex generators; total pressure recovery P_5/P_0 = 0.891; total bleed mass-flow ratio m_{btot}/m_o = 0.135; compressor face distortion D_5 = 0.214. (b) Full set of opposed generator pairs; total pressure recovery P_5/P_0 = 0.875; total bleed mass-flow ratio m_{btot}/m_o = 0.112; compressor face distortion D_5 = 0.156. (c) Conventional opposed generator pairs on cowl; total pressure recovery P_5/P_0 = 0.889; total bleed mass-flow ratio m_{btot}/m_o = 0.139; compressor face distortion D_5 = 0.145. (d) Parallel generator pairs on cowl; total pressure recovery P_5/P_0 = 0.912; total bleed mass-flow ratio m_{btot}/m_o = 0.140; compressor face distortion D_5 = 0.127. (e) Parallel generator pairs on cowl. Conventional opposed pairs on ramp; total pressure recovery, P_5/P_0 = 0.907; total bleed mass-flow rate m_{btot}/m_o = 0.113; compressor face distortion D_5 = 0.163.

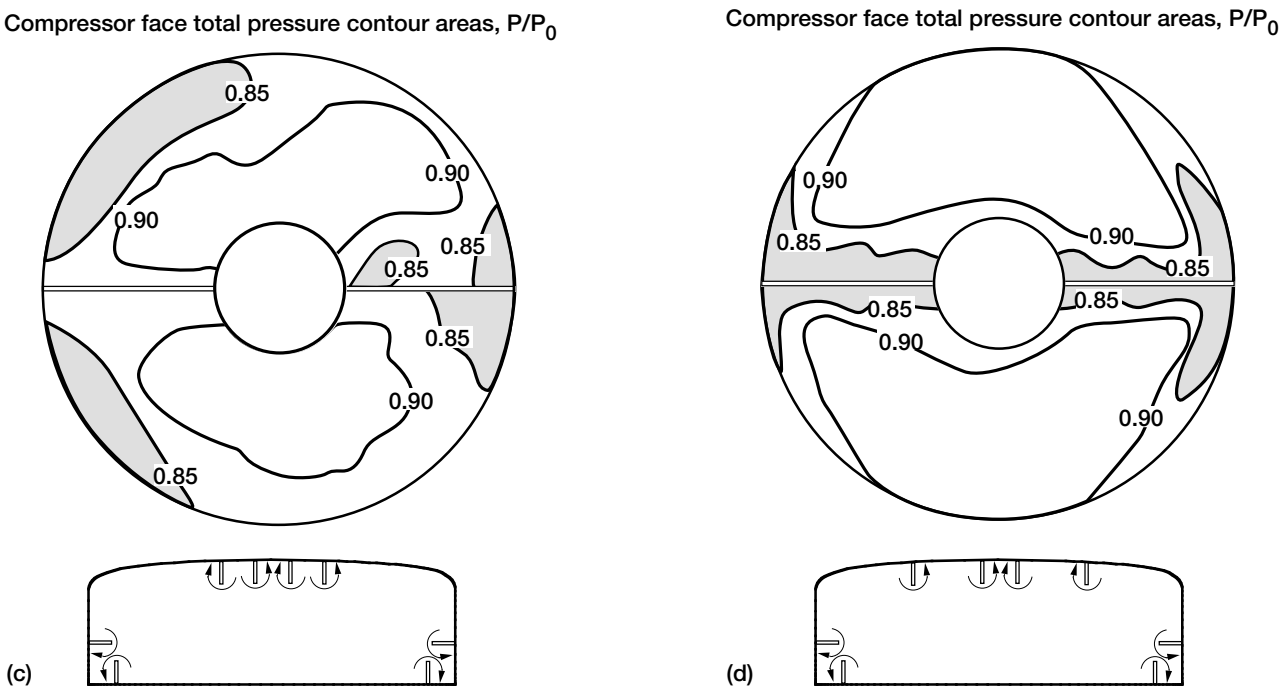

Figure 10.—Continued. (c) Conventional opposed generator pairs on cowl; total pressure recovery P_5/P_0 = 0.889; total bleed mass-flow ratio m_{btot}/m_o = 0.139; compressor face distortion D_5 = 0.145. (d) Parallel generator pairs on cowl; total pressure recovery P_5/P_0 = 0.912; total bleed mass-flow ratio m_{btot}/m_o = 0.140; compressor face distortion D_5 = 0.127.

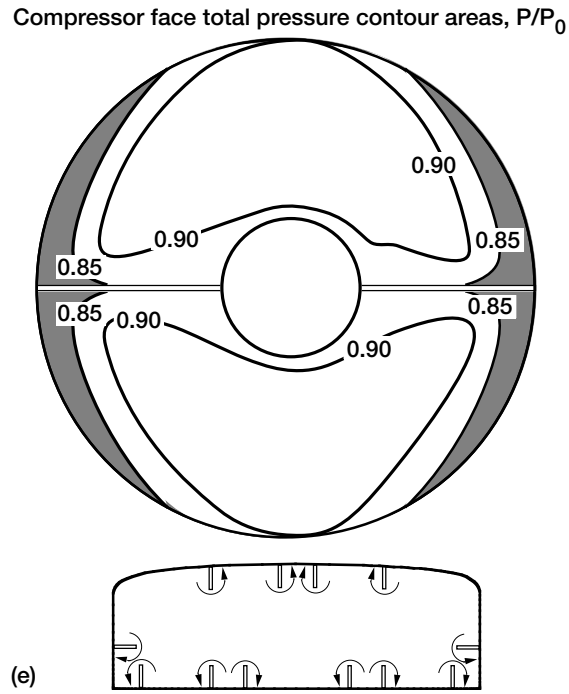

Figure 10.—Concluded. (e) Parallel generator pairs on cowl. Conventional opposed pairs on ramp; total pressure recovery, P_5/P_0= 0.907; total mass-flow rate m_{btot}/m_o = 0.113; compressor face distortion D_5 = 0.163.

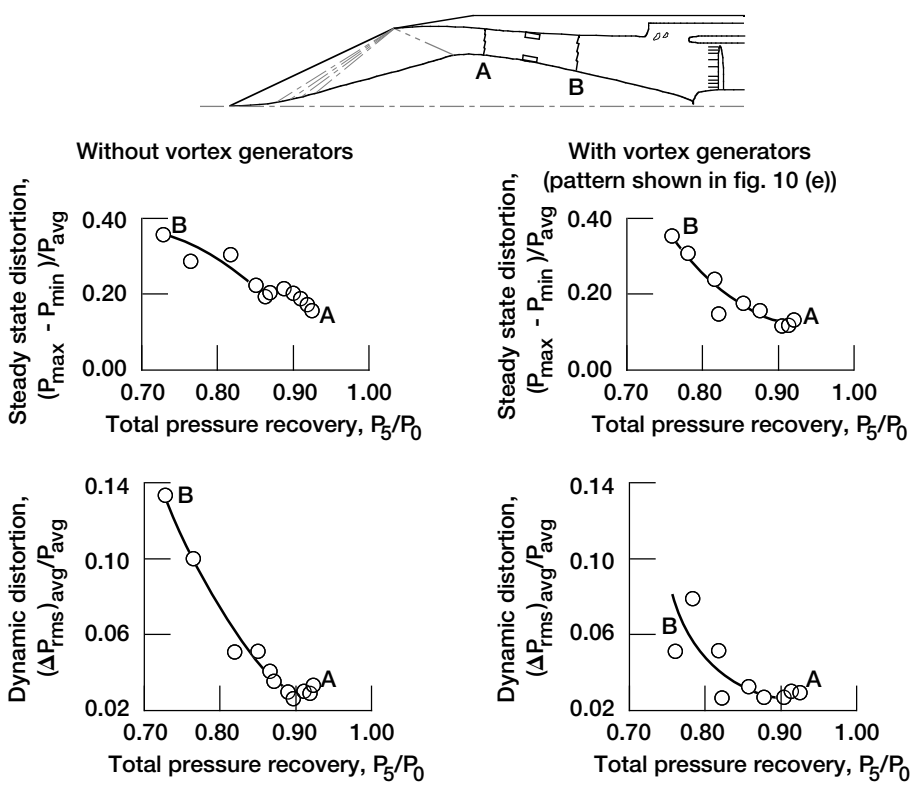

Figure 11.—Effect of vortex generators on distortion.

Bleed patterns							
			Mid-diffuser		Throat		
Configurations	Forward sidewall	Ramp shoulder	Ramp	Cowl sidewall corners	Ramp, cowl and sidewalls	Ramp corners	Cowl corners
SS-1	All exposed holes open (FS-1)	(RS-1)	(MD-4)		(Modified TB-3)		
SS-2 NSS	All exposed holes open (FS-2)	(RS-2)	(MD-3)		(TB-1)		

Vortex generator pattern for configurations SS-1, SS-2, NSS

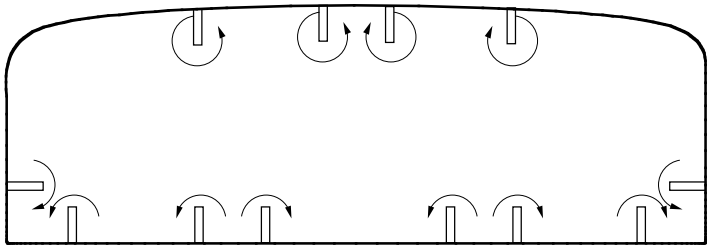

Figure 12.—Final configurations.

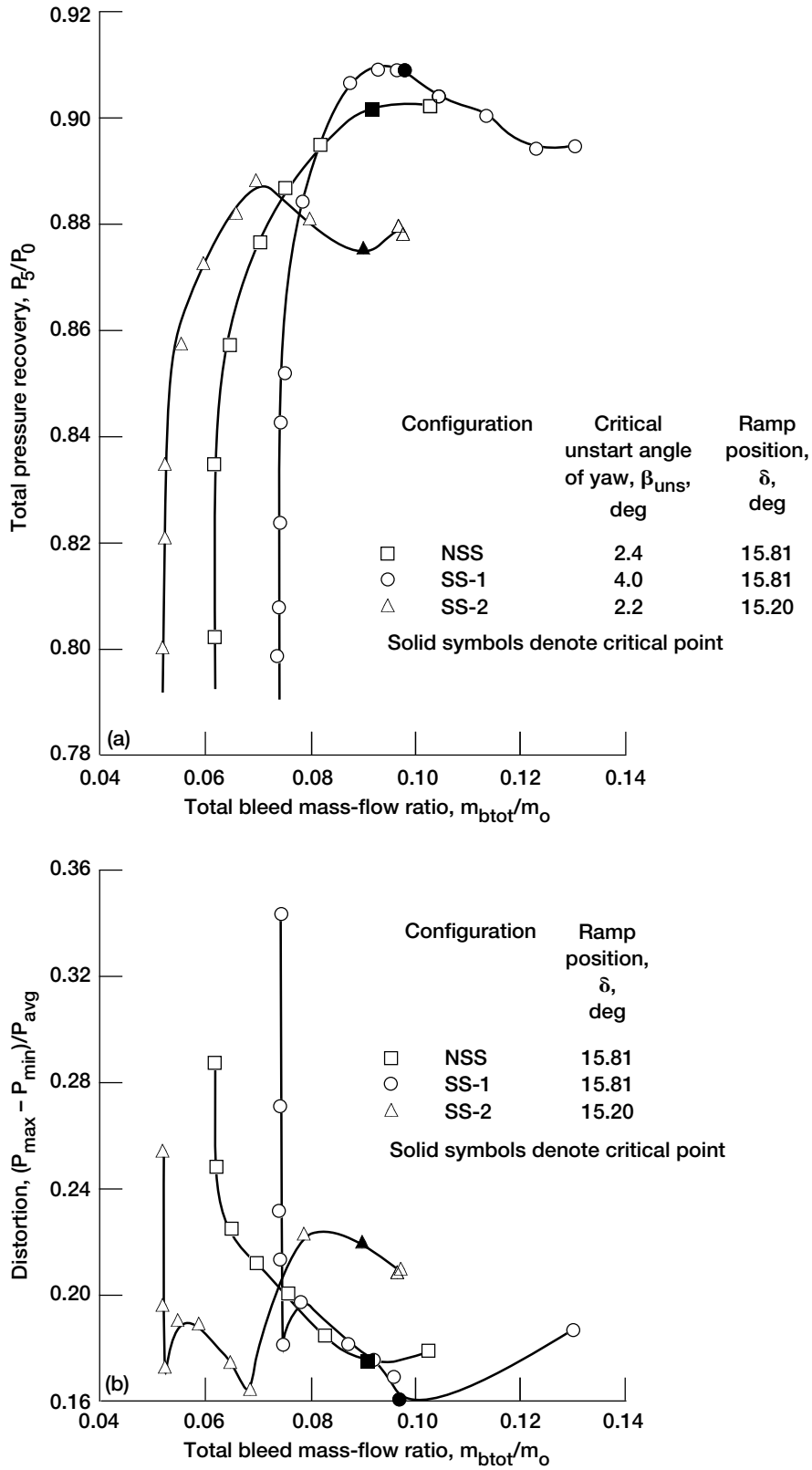

Figure 13.—Performance of final configurations at design Mach number of 2.68. (a) Total pressure recovery. (b) Inlet distortion.

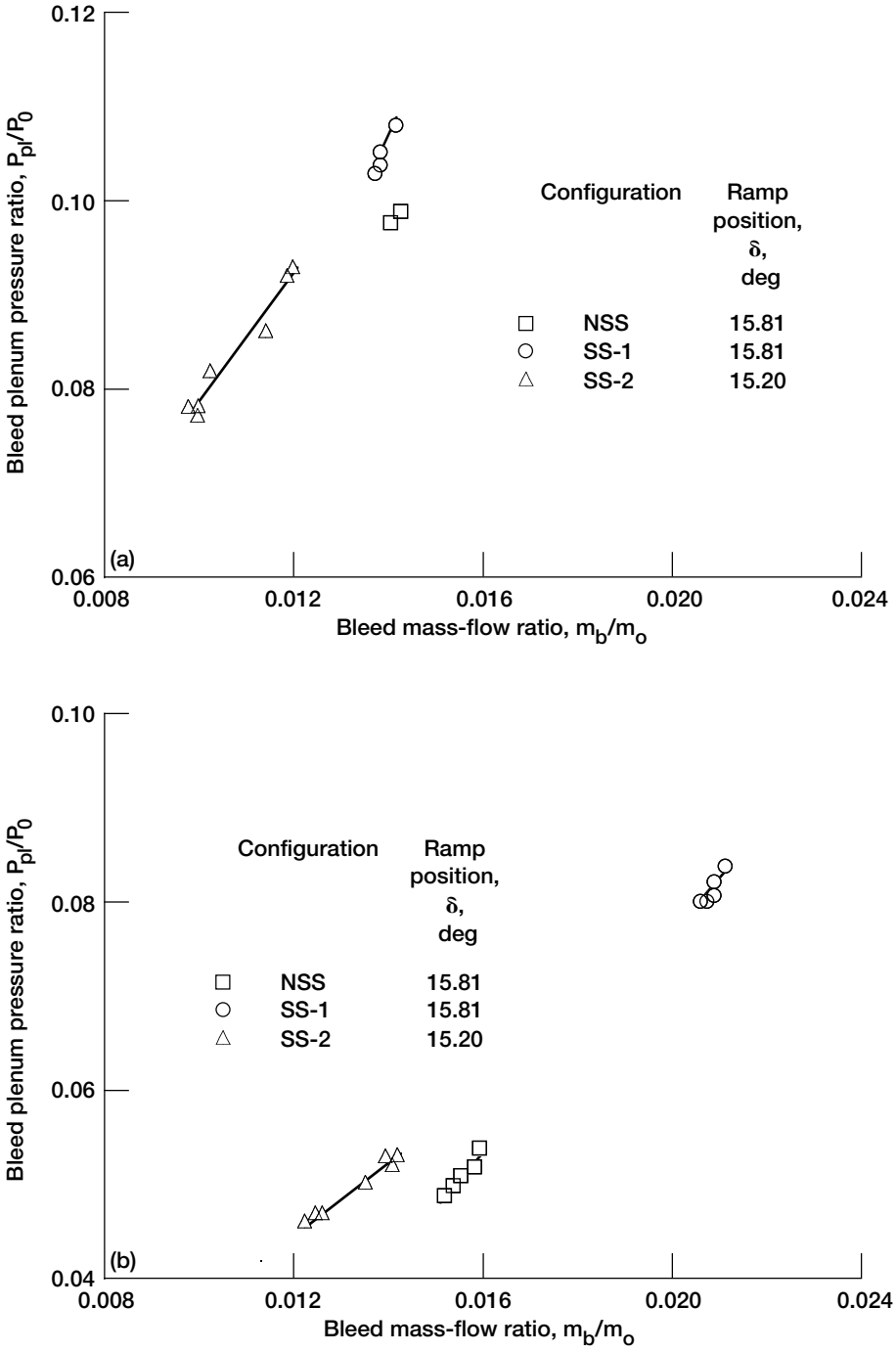

Figure 14.—Bleed system performance at design Mach number of 2.68. (a) Ramp shoulder. (b) Forward sidewall. (c) Mid-diffuser. (d) Throat.

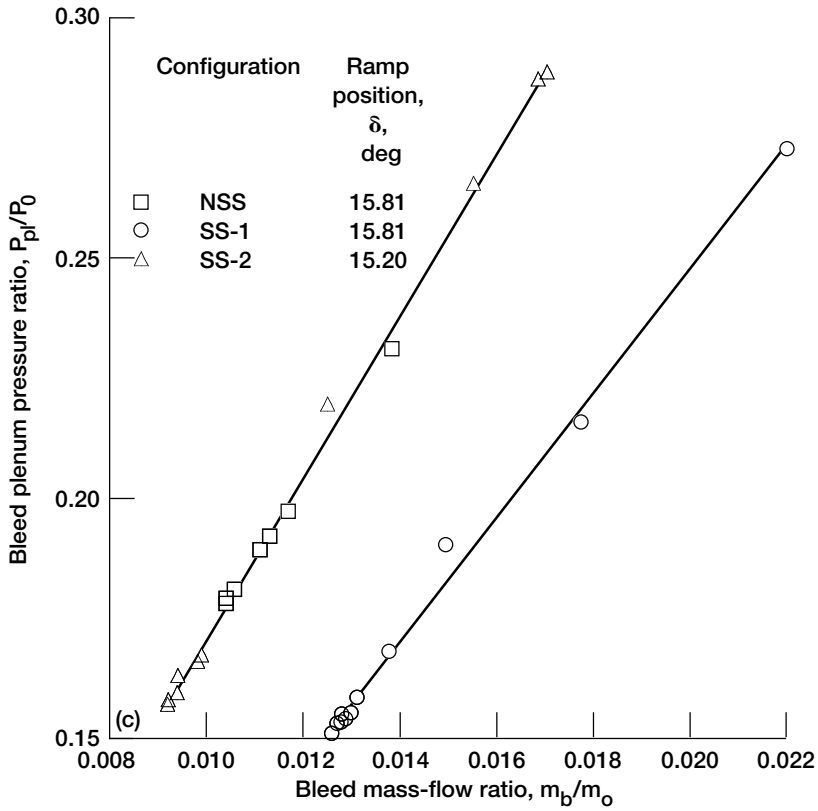

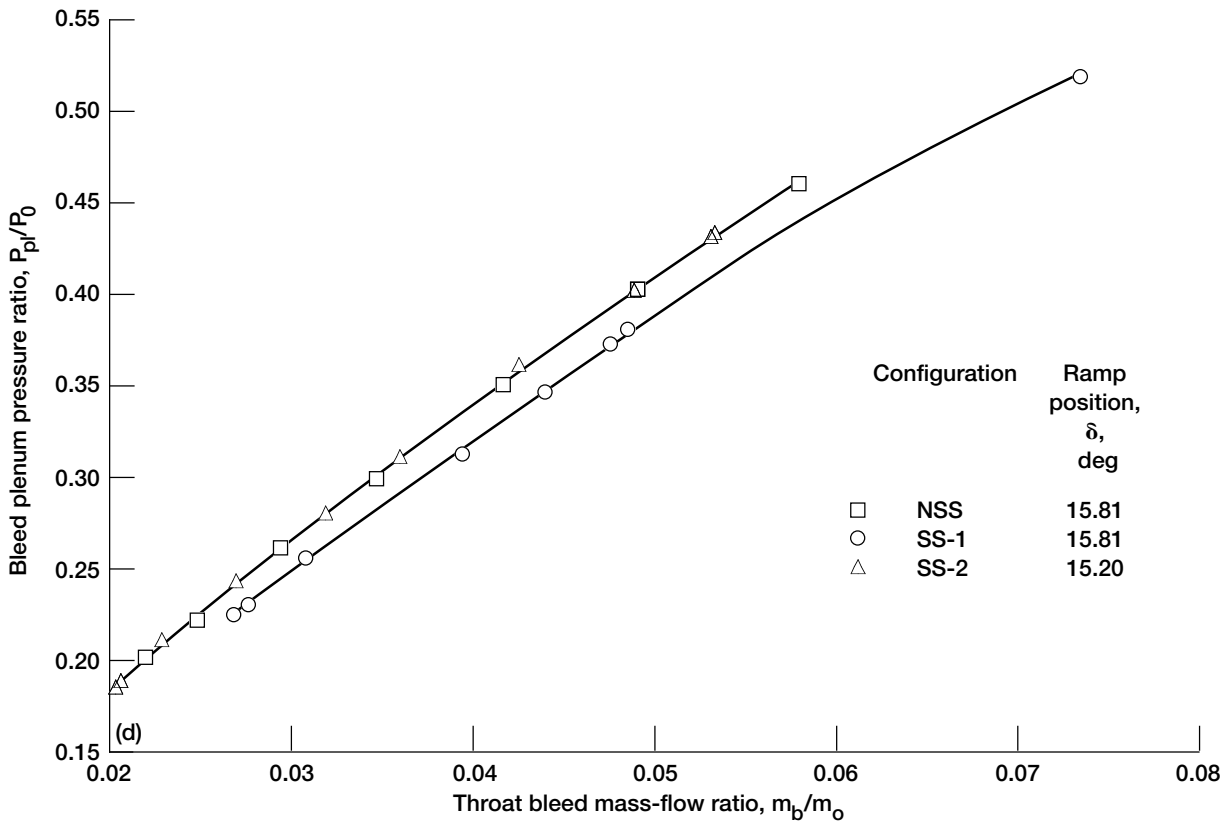

Figure 14.—Concluded. (c) Mid-diffuser. (d) Throat.

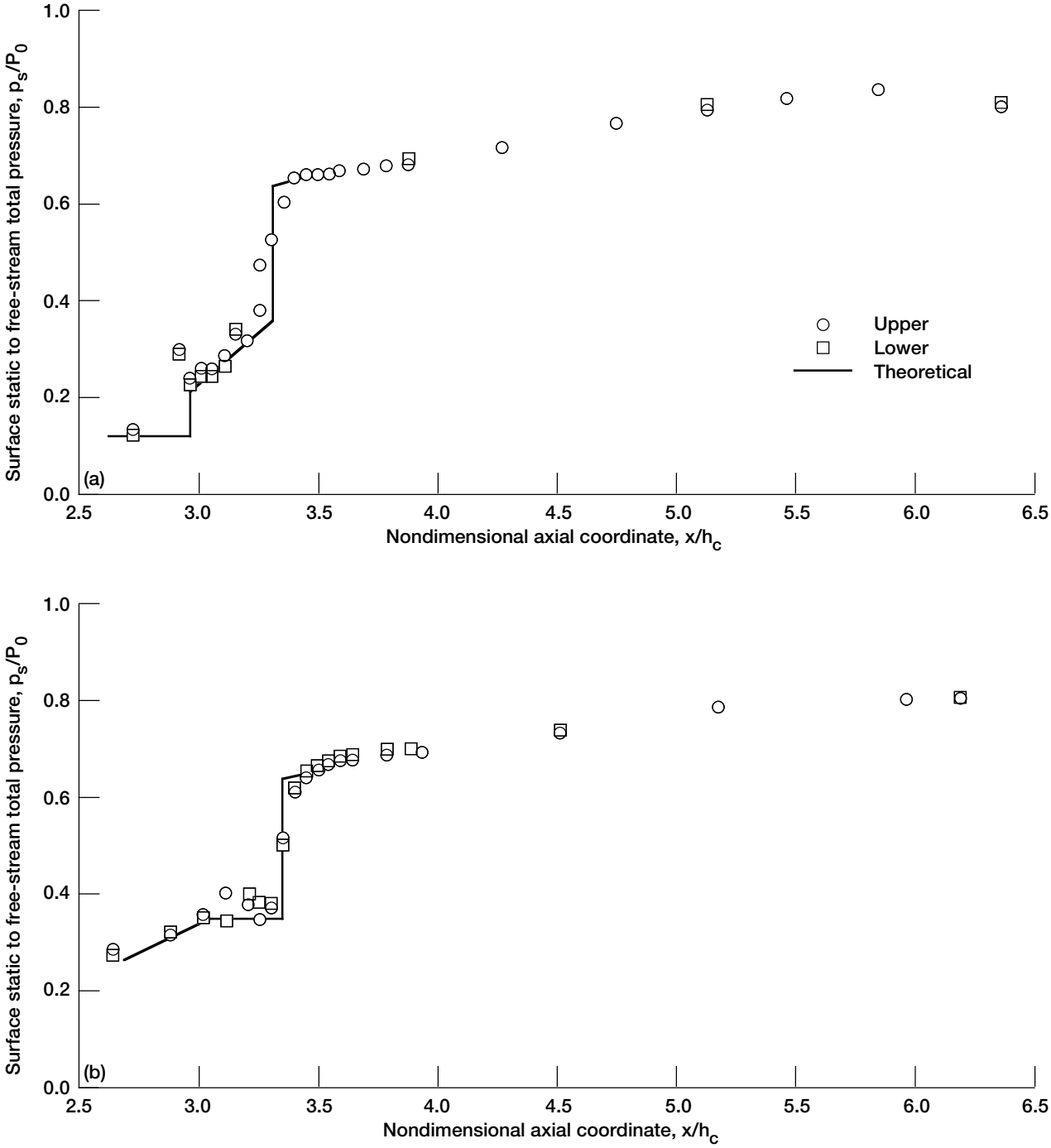

Figure 15.—Comparision of upper and lower duct static pressure profiles at design Mach number of 2.68 for configuration SS-1. Design ramp position δ = 15.81°; angle of yaw β = 0°; critical operation. (a) Ramp profile. (b) Cowl profile.

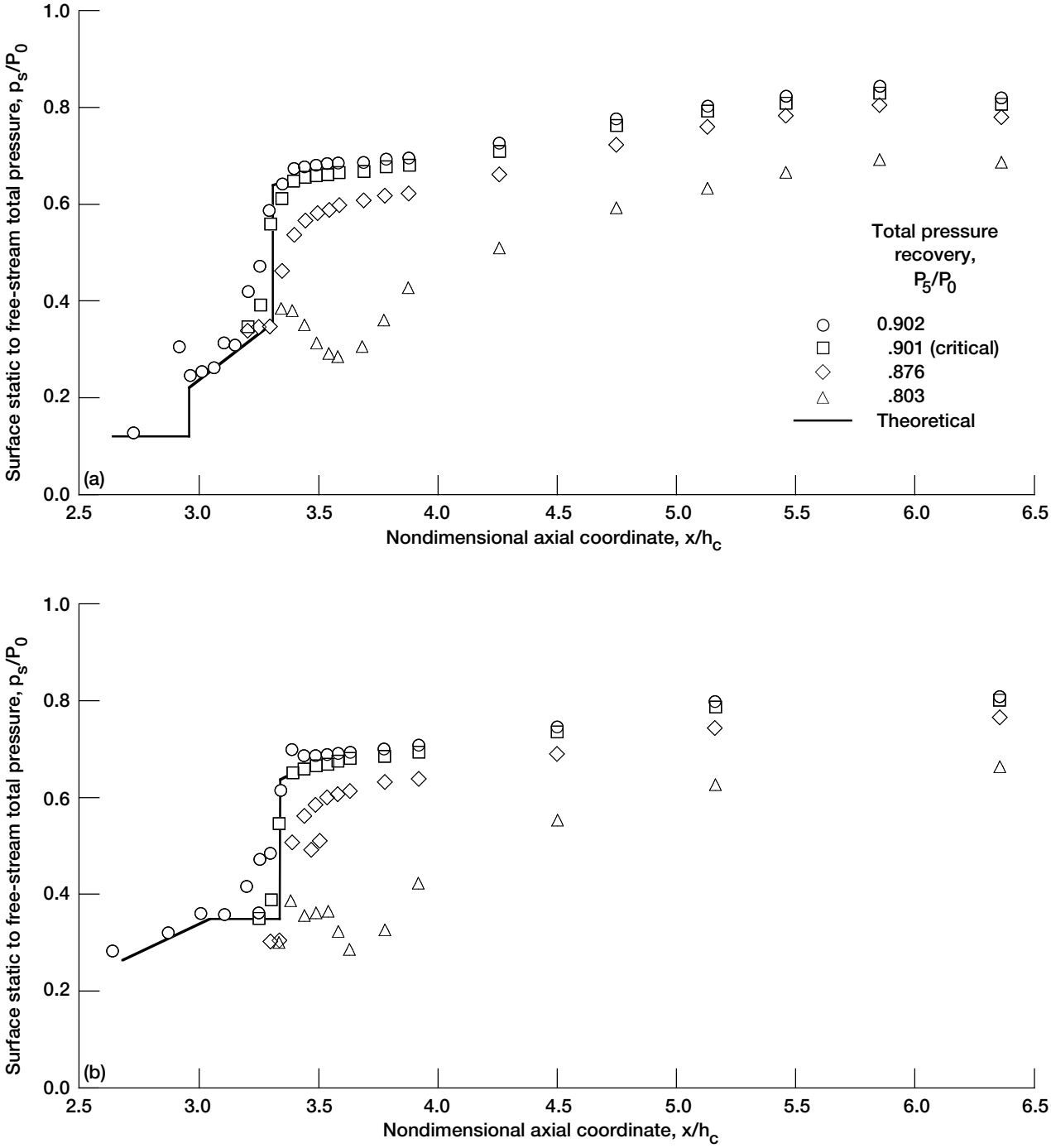

Figure 16.—Duct static pressure profiles for final configurations at design Mach number of 2.68. Design ramp position δ = 15.81°; angle of yaw β = 0°. (a) Ramp profile for NSS. (b) Cowl profile for NSS. (c) Ramp profile for SS-1. (d) Cowl profile for SS-1. (e) Ramp profile for SS-2. (f) Cowl profile for SS-2.

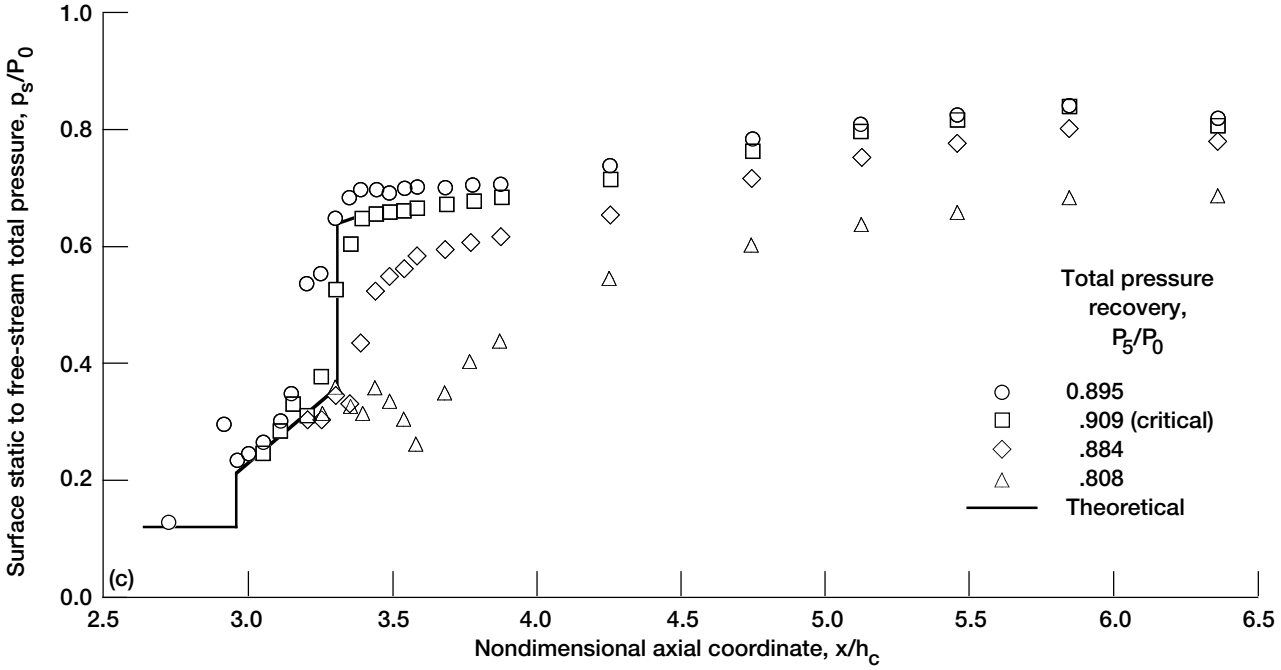

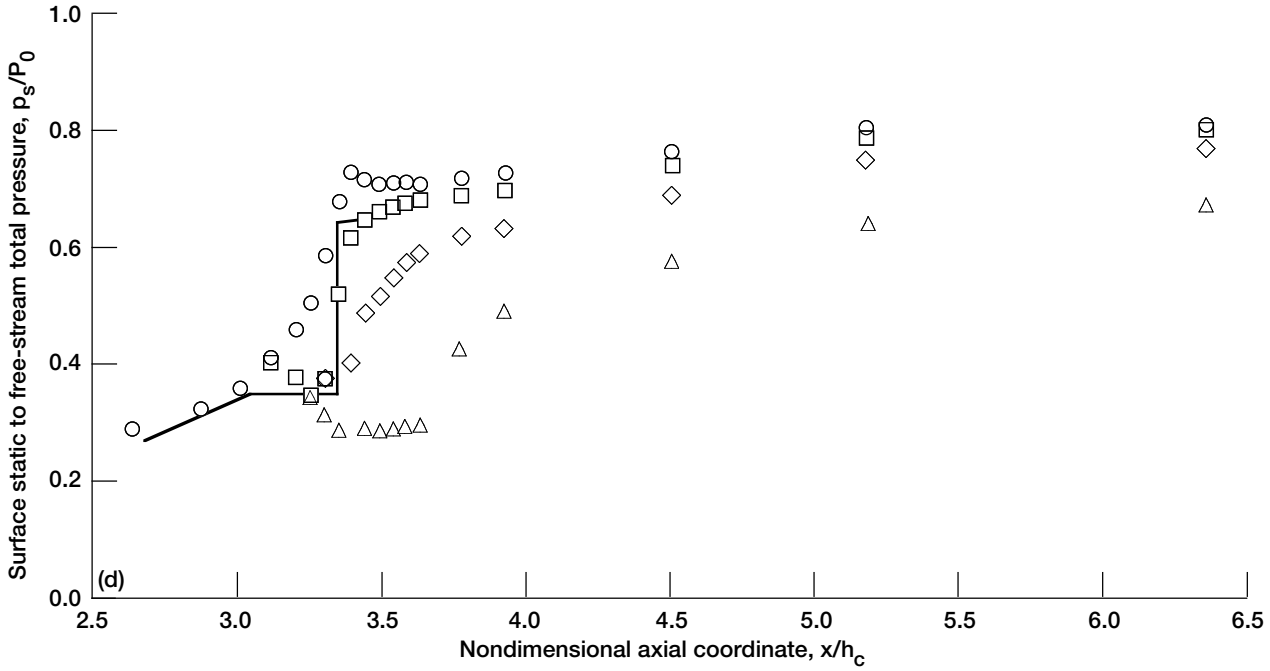

Figure 16.—Continued. (c) Ramp profile for SS-1. (d) Cowl profile for SS-1.

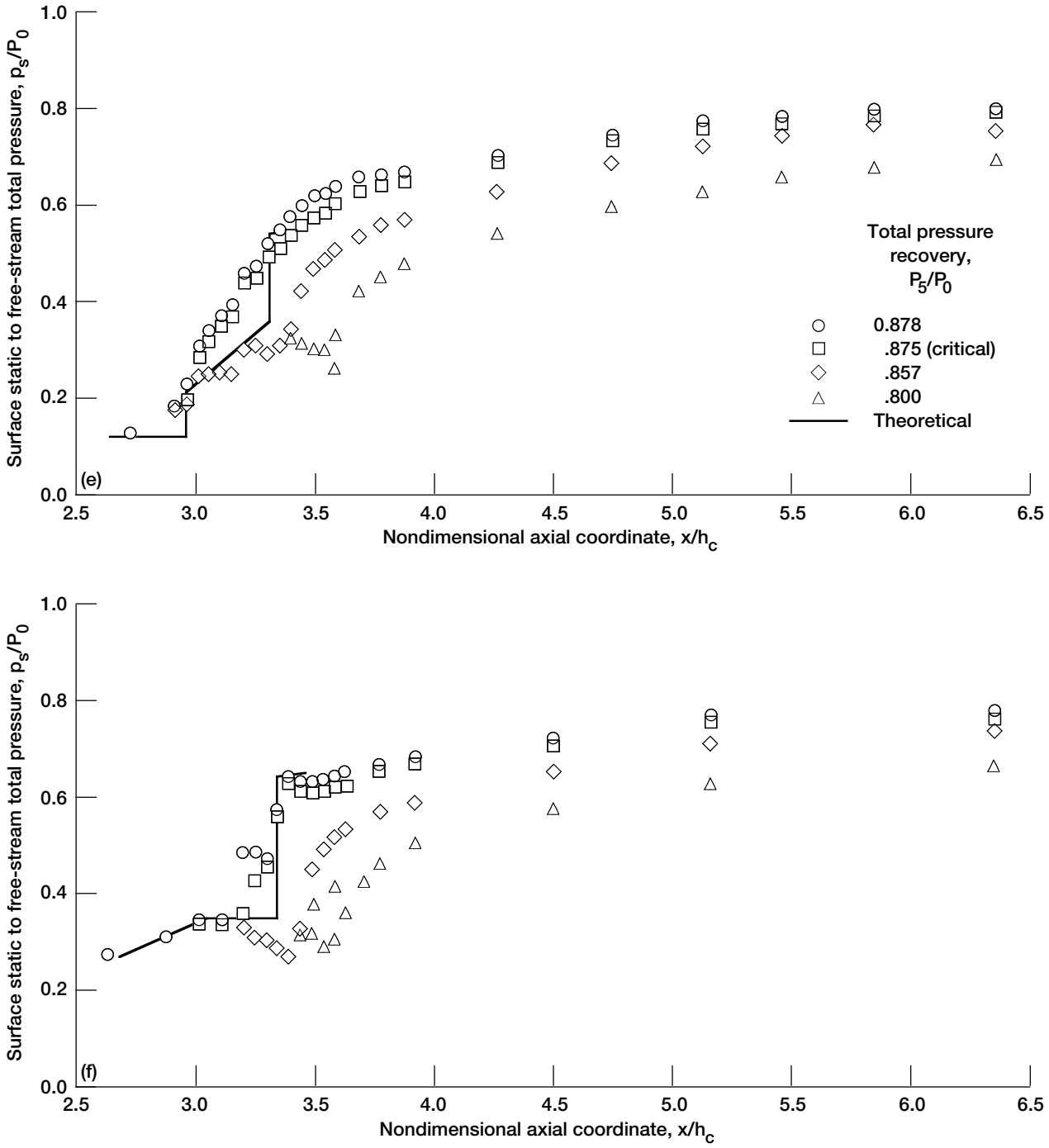

Figure 16.—Concluded. (e) Ramp profile for SS-2. (f) Cowl profile for SS-2.

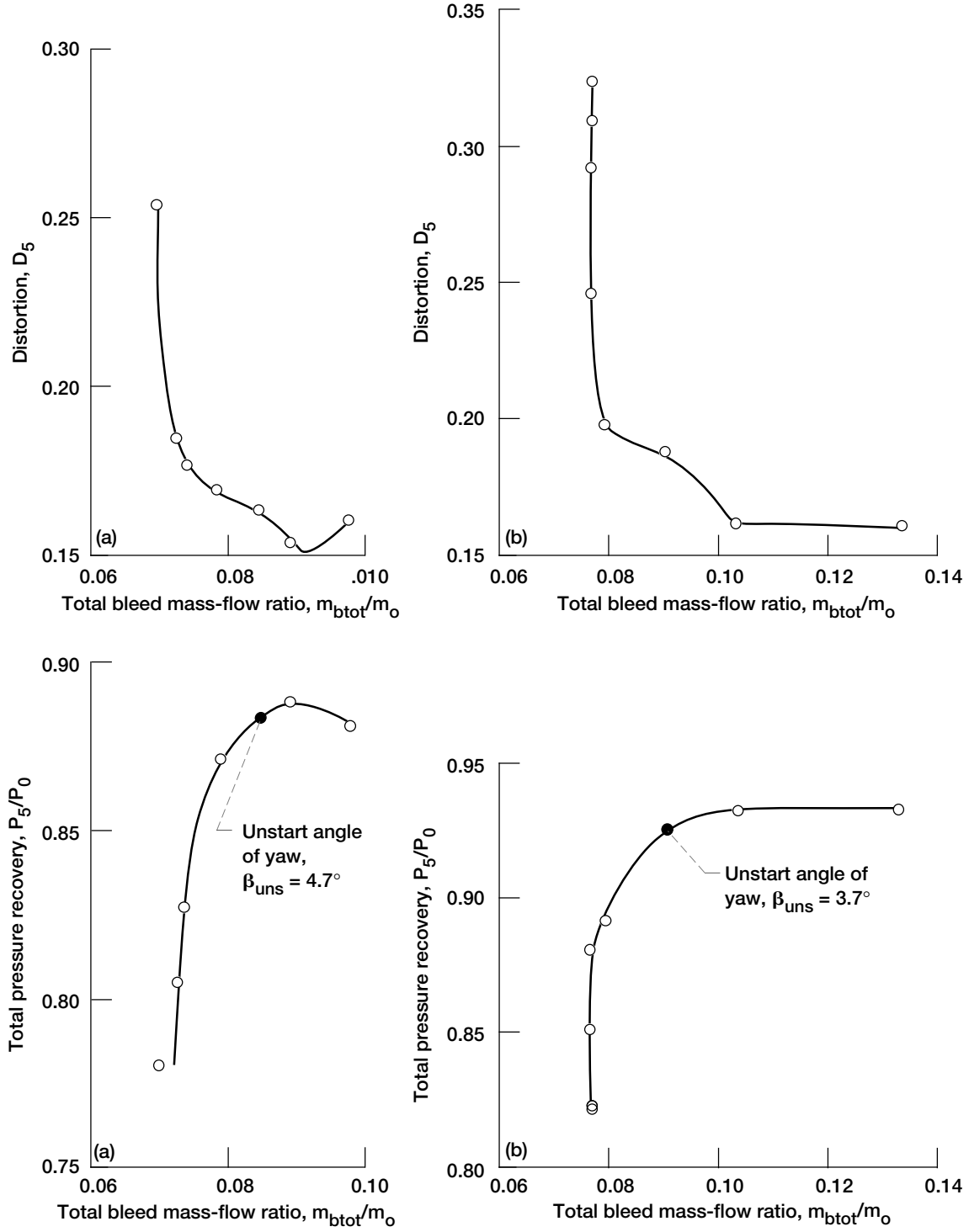

Figure 17.—Inlet performance at off-design Mach numbers. Angle of yaw $\beta = 0°$. (a) Mach number $M_0 = 2.79$; ramp position $\delta = 16.2°$, configuration SS-1. (b) Mach number $M_0 = 2.58$; ramp position $\delta = 15.4°$; configuration SS-1. (c) Mach number $M_0 = 2.50$; ramp position $\delta = 14.9°$; configuration SS-1. (d) Mach number $M_0 = 2.30$; ramp position $\delta = 13.0°$; configuration SS-1. (e) Mach number $M_0 = 2.79$; ramp position $\delta = 16.21°$; configuration SS-2. (f) Mach number $M_0 = 2.58$; ramp position $\delta = 15.13°$; configuration SS-2. (g) Mach number $M_0 = 2.50$; ramp position $\delta = 14.74°$; configuration SS-2. (h) Mach number $M_0 = 2.30$; ramp position $\delta = 12.81°$; configuration SS-2. (i) Mach number $M_0 = 2.02$; ramp position $\delta = 10.0°$; configuration SS-2.

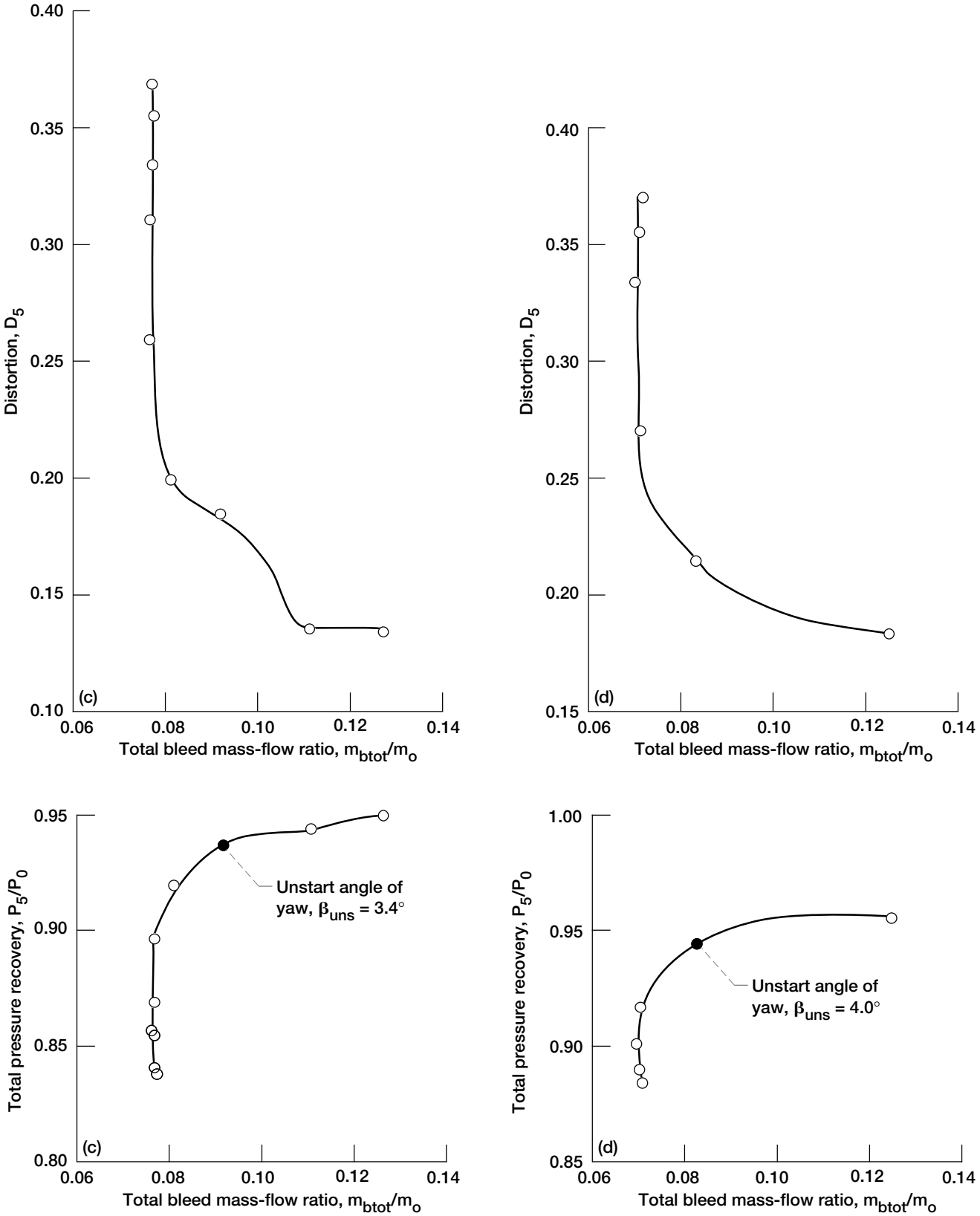

Figure 17.—Continued. (c) Mach number M_0 = 2.50; ramp position δ = 14.9°; configuration SS-1. (d) Mach number M_0 = 2.30; ramp position δ = 13.0°; configuration SS-1.

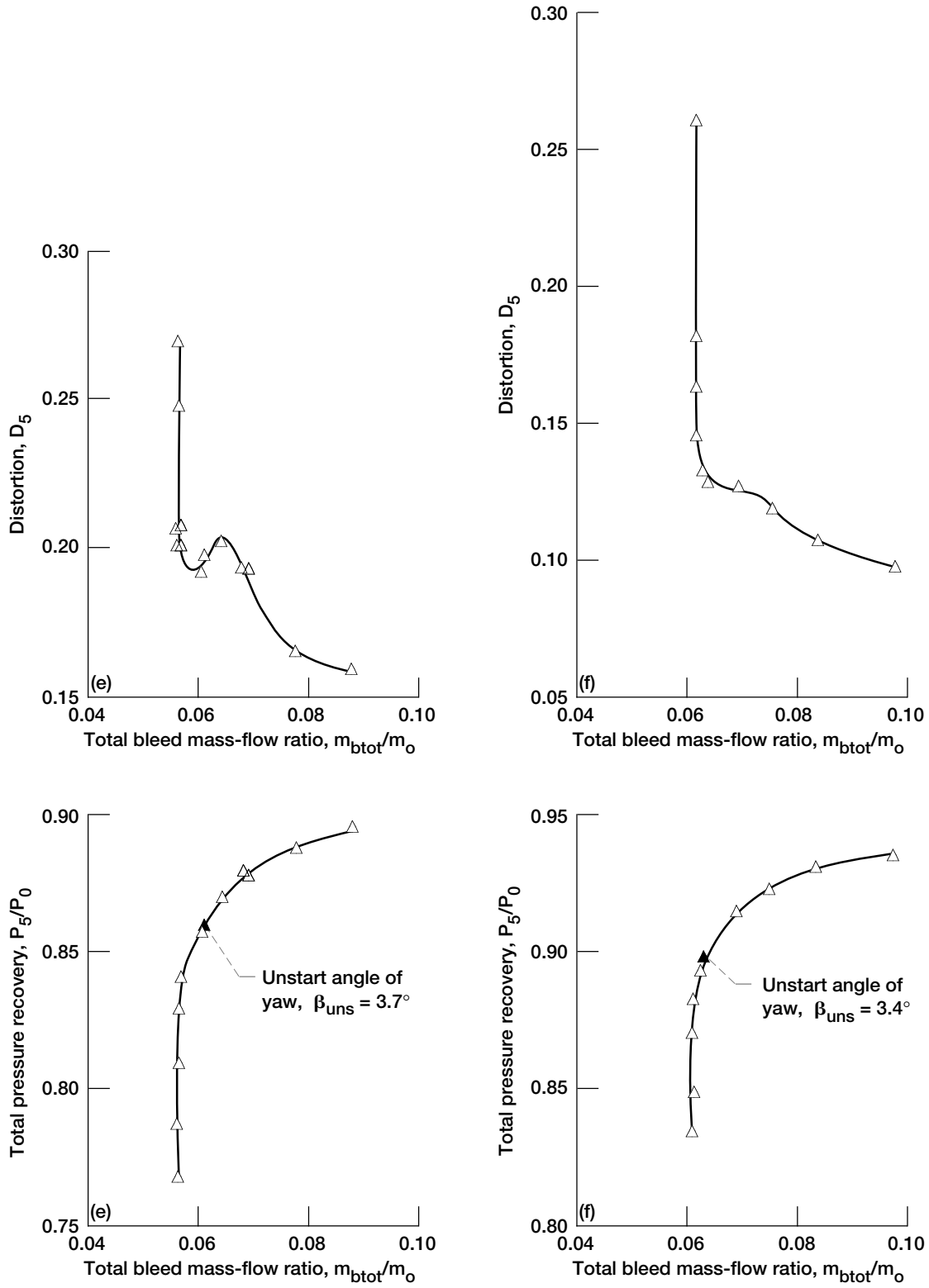

Figure 17.—Continued. (e) Mach number M_0 = 2.79; ramp position δ = 16.21°; configuration SS-2. (f) Mach number M_0 = 2.58; ramp position δ = 15.13°; configuration SS-2.

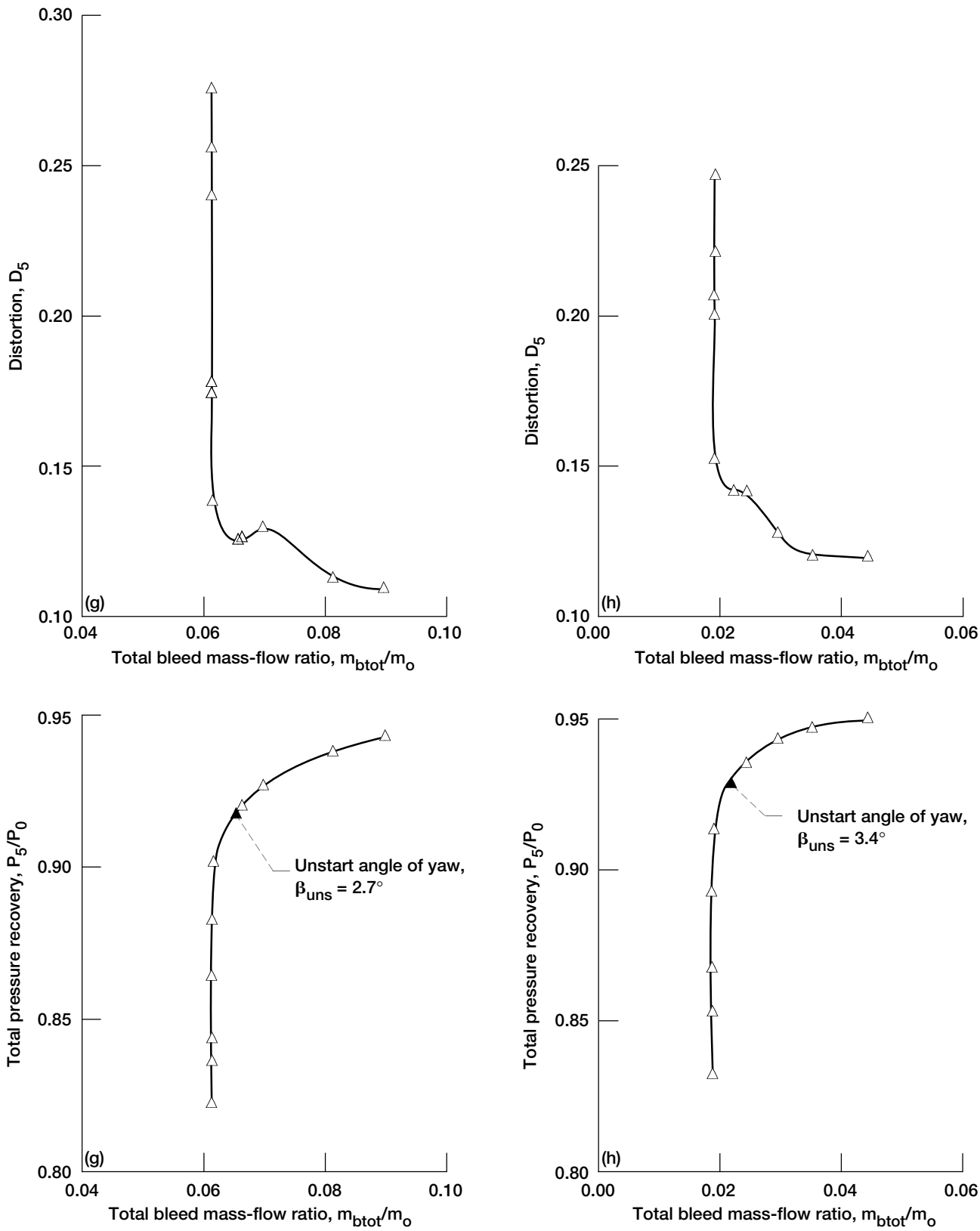

Figure 17.—Continued. (g) Mach number M_0 = 2.50; ramp position δ = 14.74°; configuration SS-2. (h) Mach number M_0 = 2.30; ramp position δ = 12.81°; configuration SS-2.

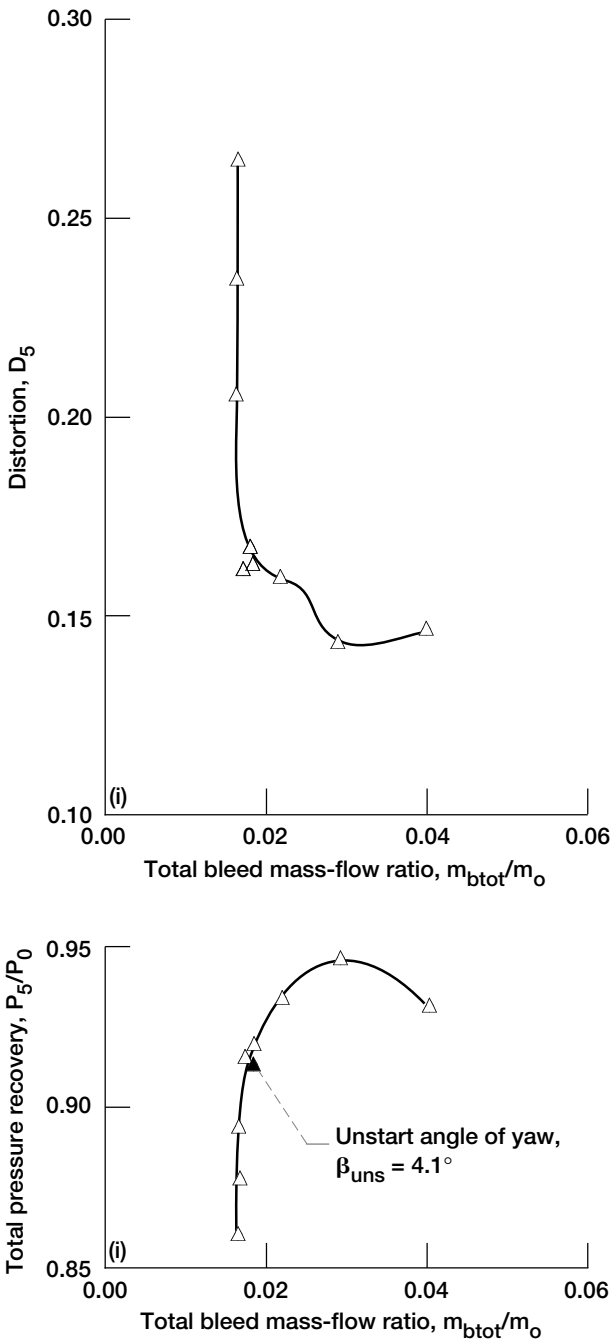

Figure 17.—Concluded. (i) Mach number M_0 = 2.02; ramp position δ = 10.0°; configuration SS-2.

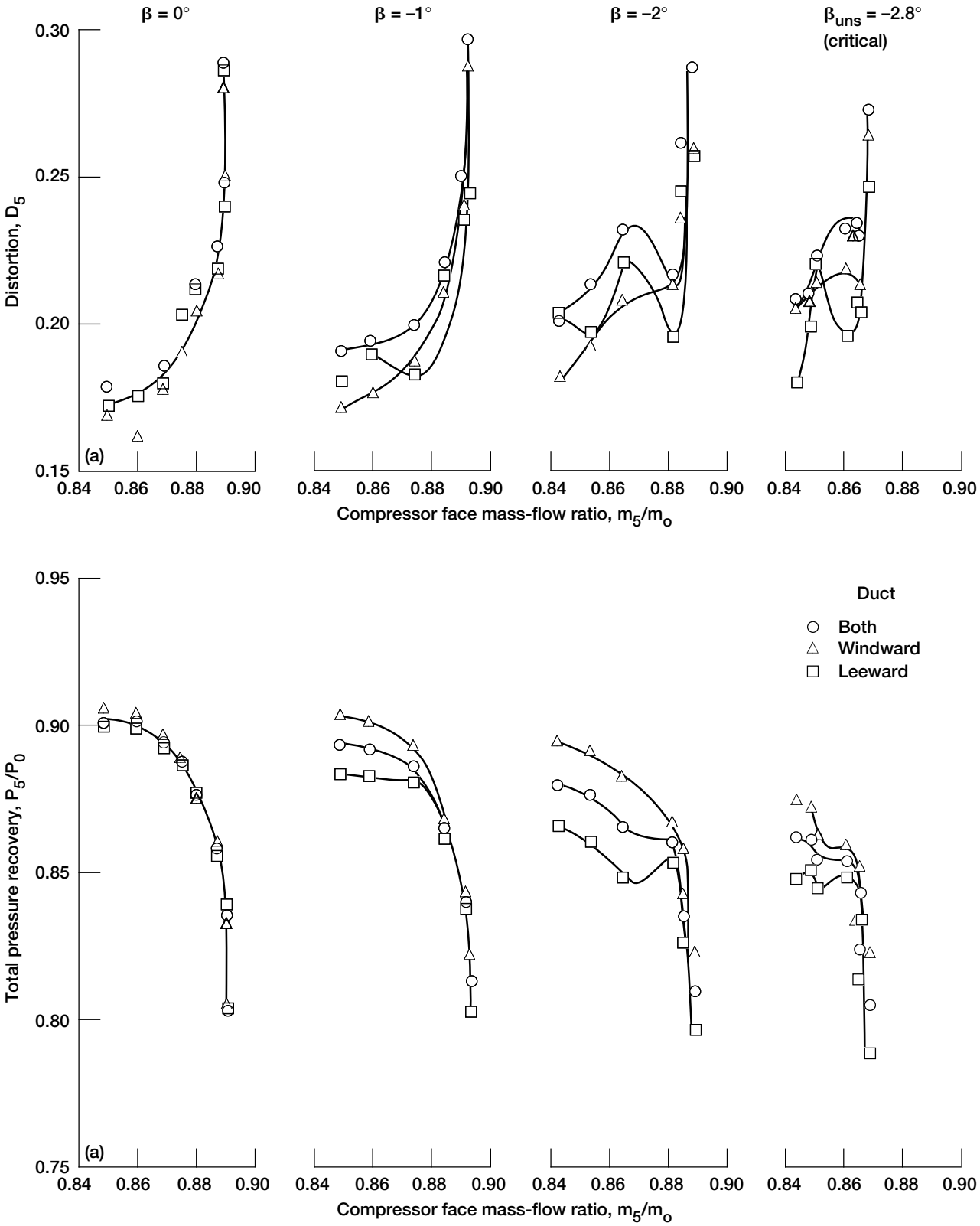

Figure 18.—Effect of yaw angle β on inlet performance at design Mach number 2.68. (a) Configuration NSS; ramp position δ = 15.81°. (b) Configuration SS-1; ramp position δ = 15.81°. (c) Configuration SS-2; ramp position δ = 15.20°.

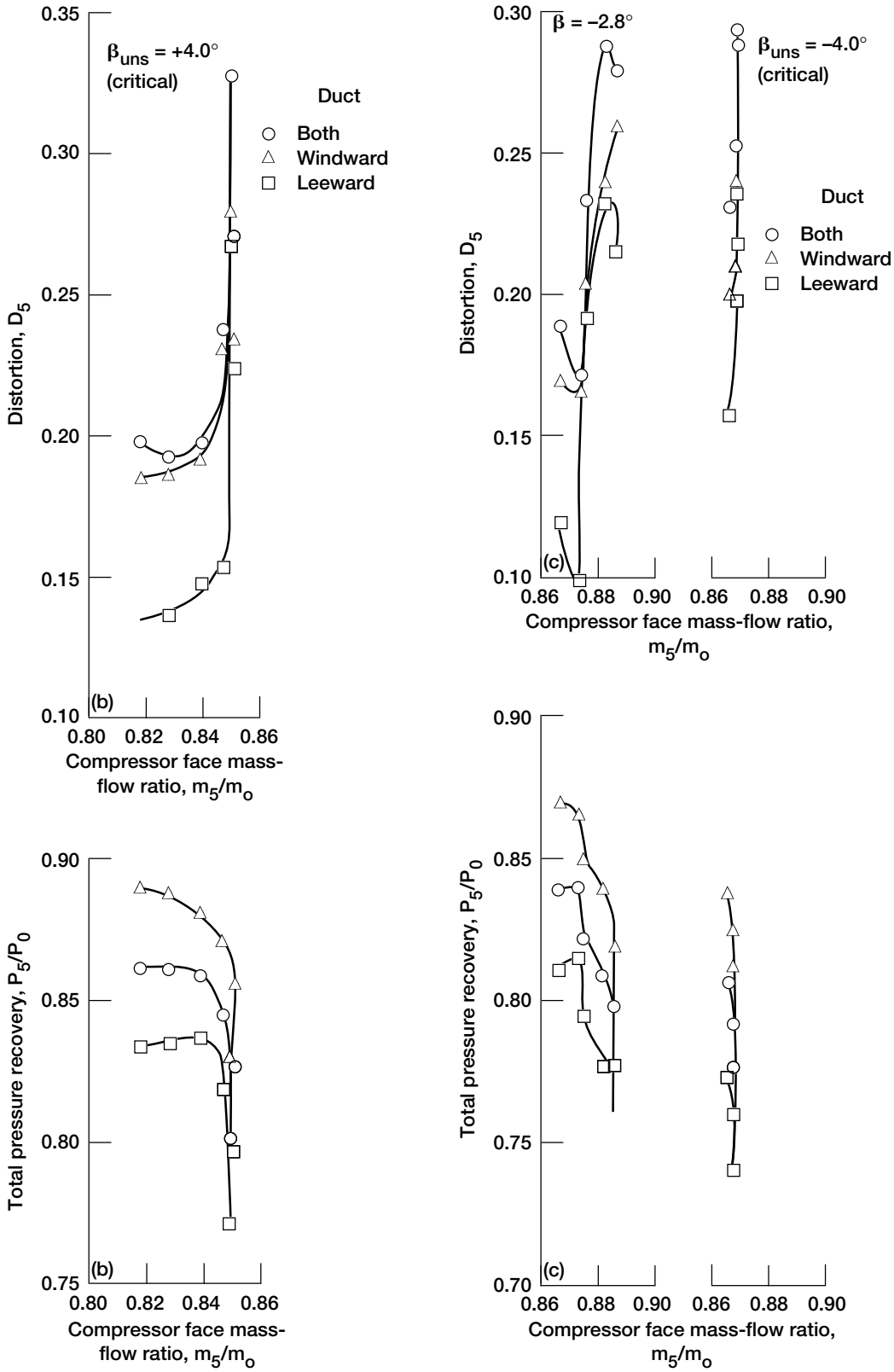

Figure 18.—Continued. (b) Configuration SS-1; ramp position δ = 15.81°. (c) Configuration SS-2; ramp position δ = 15.20°.

REPORT DOCUMENTATION PAGE

Form Approved
OMB No. 0704-0188

Public reporting burden for this collection of information is estimated to average 1 hour per response, including the time for reviewing instructions, searching existing data sources, gathering and maintaining the data needed, and completing and reviewing the collection of information. Send comments regarding this burden estimate or any other aspect of this collection of information, including suggestions for reducing this burden, to Washington Headquarters Services, Directorate for Information Operations and Reports, 1215 Jefferson Davis Highway, Suite 1204, Arlington, VA 22202-4302, and to the Office of Management and Budget, Paperwork Reduction Project (0704-0188), Washington, DC 20503.

1. AGENCY USE ONLY (*Leave blank*)

2. REPORT DATE
May 1996

3. REPORT TYPE AND DATES COVERED
Technical Memorandum

4. TITLE AND SUBTITLE
Experimental Investigation of the Performance of a Mach-2.7 Two-Dimensional Bifurcated Duct Inlet With 30 Percent Internal Contraction

5. FUNDING NUMBERS
WU–537–02–23

6. AUTHOR(S)
Joseph F. Wasserbauer, Edward T. Meleason, and Paul L. Burstadt

7. PERFORMING ORGANIZATION NAME(S) AND ADDRESS(ES)
National Aeronautics and Space Administration
Lewis Research Center
Cleveland, Ohio 44135–3191

8. PERFORMING ORGANIZATION REPORT NUMBER
E–9099

9. SPONSORING/MONITORING AGENCY NAME(S) AND ADDRESS(ES)
National Aeronautics and Space Administration
Washington, D.C. 20546–0001

10. SPONSORING/MONITORING AGENCY REPORT NUMBER
NASA TM–106728

11. SUPPLEMENTARY NOTES
Responsible person, Masashi Mizukami, organization code 2780, (216) 433–3387.

12a. DISTRIBUTION/AVAILABILITY STATEMENT
Unclassified - Unlimited
Subject Category 07

12b. DISTRIBUTION CODE

13. ABSTRACT ***(Maximum 200 words)***
An experimental study was conducted to determine the performance of a two-dimensional, mixed-compression bifurcated duct inlet system designed for a free-stream Mach number of 2.7. Thirty percent of the supersonic area contraction occurred internally. A movable ramp was used to vary the contraction ratio for off-design operation. Boundary layer bleed regions were located on the cowl, centerbody, and sidewall surfaces. There were also provisions for vortex generators on the cowl and centerbody of the subsonic diffuser. Data were obtained over the Mach number range of 2.0 to 2.8 and at angles of yaw from 0° to the maximum value prior to inlet unstart. The test at Mach 2.8 was to obtain data for an overspeed condition. The Reynolds number varied from 2.5 to 2.3 million/ft for Mach numbers above 2.5. At Mach numbers of 2.5 and lower, the Reynolds number was set at 2.5 million/ft. Bleed patterns, vortex generator patterns, and ramp position were varied, and three inlet configurations were selected for more extensive study. Two of these configurations had self-starting capability. The self-starting configuration that was developed produced 89 percent total pressure recovery at the compressor face station with 6.8 percent total bleed. The compressor face distortion was about 16 percent. Vortex generators were extremely effective in redistributing flow but were not as effective in reducing distortion. Excellent flow symmetry was achieved between the separated halves of the inlet, and twin-duct instability was not observed. The ramp tip shock was steeper than expected. This caused the cowl lip shock to be reflected from the ramp instead of being cancelled at the shoulder. However, peak recovery at the throat was still obtained with the ramp near the design position.

14. SUBJECT TERMS
Supersonic inlets; Propulsion systems

15. NUMBER OF PAGES
46

16. PRICE CODE
A03

17. SECURITY CLASSIFICATION OF REPORT
Unclassified

18. SECURITY CLASSIFICATION OF THIS PAGE
Unclassified

19. SECURITY CLASSIFICATION OF ABSTRACT
Unclassified

20. LIMITATION OF ABSTRACT